



## Assessment of the global Copernicus, NASADEM, ASTER and AW3D digital elevation models in Central and Southern Africa

Chukwuma J. Okolie, Jon P. Mills, Adedayo K. Adeleke, Julian L. Smit, Maria V. Peppas, Arif O. Altunel & Ikenna D. Arungwa

To cite this article: Chukwuma J. Okolie, Jon P. Mills, Adedayo K. Adeleke, Julian L. Smit, Maria V. Peppas, Arif O. Altunel & Ikenna D. Arungwa (01 Feb 2024): Assessment of the global Copernicus, NASADEM, ASTER and AW3D digital elevation models in Central and Southern Africa, Geo-spatial Information Science, DOI: [10.1080/10095020.2023.2296010](https://doi.org/10.1080/10095020.2023.2296010)

To link to this article: <https://doi.org/10.1080/10095020.2023.2296010>



© 2024 Wuhan University. Published by Informa UK Limited, trading as Taylor & Francis Group.



[View supplementary material](#)



Published online: 01 Feb 2024.



[Submit your article to this journal](#)



Article views: 379










[View related articles](#)



[View Crossmark data](#)

# Assessment of the global Copernicus, NASADEM, ASTER and AW3D digital elevation models in Central and Southern Africa

Chukwuma J. Okolie <sup>a,b,c</sup>, Jon P. Mills <sup>c</sup>, Adedayo K. Adeleke <sup>d</sup>, Julian L. Smit <sup>e</sup>, Maria V. Peppas <sup>c</sup>, Arif O. Altunel <sup>f</sup> and Ikenna D. Arungwa <sup>g</sup>

<sup>a</sup>Division of Geomatics, University of Cape Town, Cape Town, South Africa; <sup>b</sup>Department of Surveying and Geoinformatics, University of Lagos, Lagos, Nigeria; <sup>c</sup>School of Engineering, Newcastle University, Newcastle upon Tyne, UK; <sup>d</sup>Department of Geography, Geoinformatics and Meteorology, University of Pretoria, Pretoria, South Africa; <sup>e</sup> AfriMap Geo-information Services, Cape Peninsula University of Technology, Cape Town, South Africa; <sup>f</sup>Department of Forest Engineering, Kastamonu University, Kastamonu, Türkiye; <sup>g</sup>Department of Surveying and Geoinformatics, Federal University of Technology, Owerri, Nigeria

## ABSTRACT

Validation studies of global Digital Elevation Models (DEMs) in the existing literature are limited by the diversity and spread of landscapes, terrain types considered and sparseness of ground-truth. Moreover, there are knowledge gaps on the accuracy variations in rugged and complex landscapes, and previous studies have often not relied on robust internal and external validation measures. Thus, there is still only partial understanding and limited perspective of the reliability and adequacy of global DEMs for several applications. In this study, we utilize a dense spread of LiDAR groundtruth to assess the vertical accuracies of four medium-resolution, readily available, free-access and global coverage 1 arc-second (30 m) DEMs: NASADEM, ASTER GDEM, Copernicus GLO-30, and ALOS World 3D (AW3D). The assessment is carried out at landscapes spread across Cape Town, Southern Africa (urban/industrial, agricultural, mountain, peninsula and grassland/shrubland) and forested national parks in Gabon, Central Africa (low-relief tropical rainforest and high-relief tropical rainforest). The statistical analysis is based on robust accuracy metrics that cater for normal and non-normal elevation error distribution, and error ranking. In Cape Town, Copernicus DEM generally had the least vertical error with an overall Mean Error (ME) of 0.82 m and Root Mean Square Error (RMSE) of 2.34 m while ASTER DEM had the poorest performance. However, ASTER GDEM and NASADEM performed better in the low-relief and high-relief tropical forests of Gabon. Generally, the DEM errors have a moderate to high positive correlation in forests, and a low to moderate positive correlation in mountains and urban areas. Copernicus DEM showed superior vertical accuracy in forests with less than 40% tree cover, while ASTER and NASADEM performed better in denser forests with tree cover greater than 70%. This study is a robust regional assessment of these global DEMs.

## ARTICLE HISTORY

Received 20 March 2023  
Accepted 11 December 2023

## KEYWORDS

Global digital elevation model; NASADEM; ASTER; ALOS World 3D; Copernicus; LiDAR; NASA Land Vegetation and Ice Sensor (LVIS); height error map

## 1. Introduction

The periodic release of open-access global Digital Elevation Models (DEMs) has given rise to numerous calibration and validation studies devoted to understanding their qualities and performance limitations (e.g. Ebinne et al. 2022; Nwilo et al. 2022). This knowledge is important for precise application of global DEMs in different fields of endeavor. Moreover, global DEMs have varying spatial resolutions and temporal coverages, and are the result of different acquisition techniques. This leads to inconsistencies in their qualities including geometric characteristics, accuracy levels and hydro-geomorphological characteristics. The concept of quality is much broader, but is most often assimilated to the vertical accuracy of the DEM (Mesa-Mingorance and Ariza-López 2020). Despite

the growing body of knowledge on DEM validation, numerous assessments have been limited by the diversity and spread of groundtruth particularly in challenging or inaccessible environments such as dense forests and mountainous terrain (Oliveira, Paradella, and Silva 2011). The consequence of this is a limited perspective of the vertical accuracies of global DEMs for applications such as hydrological, environmental and topographic modeling. Thus, there is a necessity for more studies on the vertical accuracy and performance limitations of global DEMs in different landscapes.

More than two decades ago, the National Aeronautics and Space Administration (NASA) and other global partners commenced the data acquisition for two of the foremost global DEMs, which were

**CONTACT** Chukwuma J. Okolie  drcjokolie@gmail.com

 Supplemental data for this article can be accessed online at <https://doi.org/10.1080/10095020.2023.2296010>.

© 2024 Wuhan University. Published by Informa UK Limited, trading as Taylor & Francis Group.

This is an Open Access article distributed under the terms of the Creative Commons Attribution License (<http://creativecommons.org/licenses/by/4.0/>), which permits unrestricted use, distribution, and reproduction in any medium, provided the original work is properly cited. The terms on which this article has been published allow the posting of the Accepted Manuscript in a repository by the author(s) or with their consent.

subsequently released to worldwide users. These two DEMs are the Shuttle Radar Topography Mission (SRTM) DEM (C-band and X-band radar) and the Advanced Spaceborne Thermal Emission and Reflection Radiometer (ASTER) DEM (Abrams, Crippen, and Fujisada 2020; Rabus et al. 2003). Recently, the original SRTM radar measurements have been reprocessed by NASA to generate an updated version referred to as NASADEM version 1 which was released in 2020, whereas the most recent version of ASTER (version 3) was released in 2019. Although both SRTM and ASTER have undergone several developmental phases, their data acquisition periods may be several years behind newer global DEMs such as the Advanced Land Observing Satellite (ALOS) World 3D DEM (AW3D) (initially released in 2019) and the Copernicus GLO-30 DEM (released in 2020). It is important to note that NASADEM, ASTER, Copernicus and AW3D are surface models i.e. they are representative of both the “bare ground” surface and above-ground features (e.g. buildings and trees).

The accuracy of DEMs is key to a myriad of applications including climate change (Bove et al. 2020), flood and sea level rise modeling (Gesch 2018; Hooijer and Vernimmen 2021; McClean, Dawson, and Kilsby 2020; Muthusamy et al. 2021; Xu et al. 2021), glacier mass balance and volume change assessment (Barrand et al. 2009; Chen et al. 2022; Friedt et al. 2012; McNabb et al. 2019; Yan, Wang, and Shao 2022), assessment of volcanic flows (Sánchez et al. 2022; Stevens, Manville, and Heron 2003), monitoring rockfalls and landslides (Kakavas and Nikolakopoulos 2021; Rabby, Ishtiaque, and Rahman 2020), mapping of geological lineaments (Florinsky 2008), groundwater modeling (Ishola et al. 2023), crustal deformation monitoring (Epuh et al. 2022), hydrological and hydrographic analysis (e.g. HydroSHEDS; Lehner, Verdin, and Jarvis 2008) and geomorphometric analysis (Banerjee, Santhosh Kumar, and Tilak 2022; Kasi et al. 2020; Nwilo et al. 2021). A literature survey shows a plethora of accuracy assessment studies comparing global DEMs. For example, Uuemaa et al. (2020) examined the accuracy of several global DEMs including ASTER GDEM v2, AW3D30 and NASADEM in regions with different topography and land cover. After several tests, they concluded that AW3D30 displayed the most stable performance. However, their study was limited because of the use of a 100 m global land cover dataset which is lower than the resolution of the analyzed DEMs. In another study covering vegetated and “high-relief” terrain, Guth and Geoffroy (2021) evaluated the height distribution of NASADEM, ASTER, Copernicus and AW3D. They asserted the superiority of Copernicus DEM in tests against both LiDAR and Ice, Cloud, and land Elevation Satellite (ICESat-2) data. Li et al. (2022) investigated the accuracy of the

30 m Copernicus, NASADEM and AW3D30 in selected terrains of China, using high-quality ICESat-2 validation points. Their results indicated the three DEMs had similar overall vertical accuracy, with Root Mean Square Error (RMSE) of 6.73 m (Copernicus), 6.59 m (NASA) and 6.63 m (AW3D30). NASADEM and AW3D30 performed better in steep areas while Copernicus DEM performed better in low-relief areas.

Nonetheless, systematic external accuracy assessments of the most recent versions of all four global DEMs (i.e. NASADEM v001, ASTER GDEM v3, Copernicus GLO-30 and AW3D v3.2) in landscapes with variable topography (e.g. high-relief, low-relief) and land cover (urban and industrial areas, grasslands, shrublands and dense thickets, tropical forests, agricultural fields) are still required. Also, often-overlooked internal validation methods such as visual inspection are required for a well-rounded analysis. Lastly, due to their recent release, accuracy assessments of NASADEM and Copernicus DEM are still limited. Scientists, researchers and the global community of end-users are still in need of a comprehensive and multi-perspective analysis of these frontline global DEMs, i.e. NASADEM, ASTER GDEM, Copernicus and AW3D. This study addresses the following research questions:

- What are the vertical accuracies of the most recent versions of NASADEM, ASTER, Copernicus and AW3D DEMs, based on very accurate reference data?
- How does the vertical accuracy of these DEMs differ in urban/industrial, agricultural, mountainous, peninsula, grassland/shrubland and forested landscapes?
- How does DEM accuracy vary in relation to percentage tree cover?
- How do terrain parameters (slope and aspect) influence the vertical accuracy of the selected DEMs?

To answer these questions, we combine qualitative and quantitative analytical approaches for assessing the vertical accuracy of the four DEMs using two high-resolution airborne LiDAR datasets from the City of Cape Town (2023) and the AfriSAR Land Vegetation and Ice Sensor Level 2 Geolocated Surface Elevation Product for Gabon (Fatoyinbo et al. 2021). The error assessment is conducted at seven sites located in Cape Town (South Africa), Akanda National Park (North-west Gabon) and Lopé National Park (Central Gabon).

## 2 Methodology

The vertical accuracy of DEMs is influenced by several factors such as the nature of the terrain. An adequate

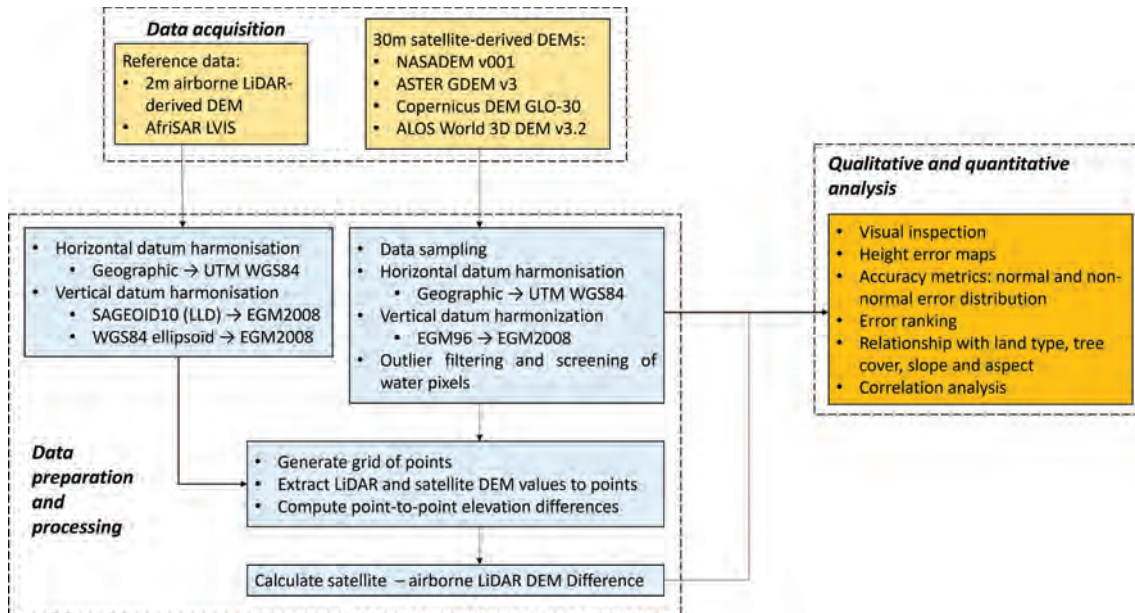


Figure 1. Workflow diagram of the assessment methodology.

accuracy assessment of DEMs should consider several factors including the spatial distribution of ground control points, DEMs of difference and terrain derivatives (Carrera-Hernández 2021; Höhle and Höhle 2009). Figure 1 presents a workflow diagram of the methodology.

## 2.1. Study area

Seven landscapes (shown in Figures 2 and 3) were selected for the study. The sites are exceptionally diverse in terms of land cover and topography, providing a wide spectrum of geomorphological contexts well suited for the presented study. Table 1 lists the site descriptions. We chose sites where LiDAR data was available and where different terrain conditions (e.g. mountainous, peninsula, flat) coexisted with various land cover types (e.g. agricultural land, urban/industrial, forests).

### 2.1.1. Cape Town, South Africa

Cape Town is South Africa's most south-western city, with a land cover area of about 400 km<sup>2</sup> (Orimoloye et al. 2019). It is situated on the south-western coast of the Western Cape Province. The coastline varies from sandy to rocky, to steep and mountainous. Cape Town has a high landscape-level diversity (Goodness and Anderson 2013).

### 2.1.2. Akanda and Lopé National Parks, Gabon

Equatorial rain forests cover approximately 85% of Gabon (Hille 2016; WRM 2013). The country is physically characterized by a narrow coastal plain and a hilly interior. It has a total area coverage of 267,667 km<sup>2</sup> (Goldstein et al. 2017) whereby 257,667 km<sup>2</sup> is land area and 10,000 km<sup>2</sup> is water area. Two

forested national parks, Akanda (North-west Gabon) and Lopé (Central Gabon) were selected for this study.

## 2.2. Datasets

The 1 arc-second (30 m spatial resolution) DEMs assessed in this study are presented together with their characteristics in Table 2. These DEMs were derived using either Synthetic Aperture Radar interferometry (InSAR) or stereo-photogrammetry (optical), each with its own merits and limitations. The reference DEMs adopted are the airborne LiDAR DEM of Cape Town City, and the AfriSAR Land Vegetation and Ice Sensor (LVIS) Level 2 Geolocated Surface Elevation Product. The specific tile IDs used are shown in Table 3.

### 2.2.1. NASADEM v001

NASADEM is an update of the DEM and associated products generated from the SRTM data (Buckley et al. 2020). SRTM was a joint venture between NASA, the National Geospatial-Intelligence Agency (NGA), the German Aerospace Centre (DLR) and the Italian Space Agency (ASI). The original SRTM raw signal radar data was reprocessed using improved algorithms, and further improvements were made through the incorporation of additional data from ASTER and ICESat – Geoscience Laser Altimeter System (GLAS) instruments. Through improvements in phase unwrapping and the use of ICESat GLAS data for control, a significant reduction in voids was achieved in NASADEM (Buckley et al. 2020).

### 2.2.2. ASTER GDEM v3

The ASTER Global DEM is the result of a collaboration between NASA and the Ministry



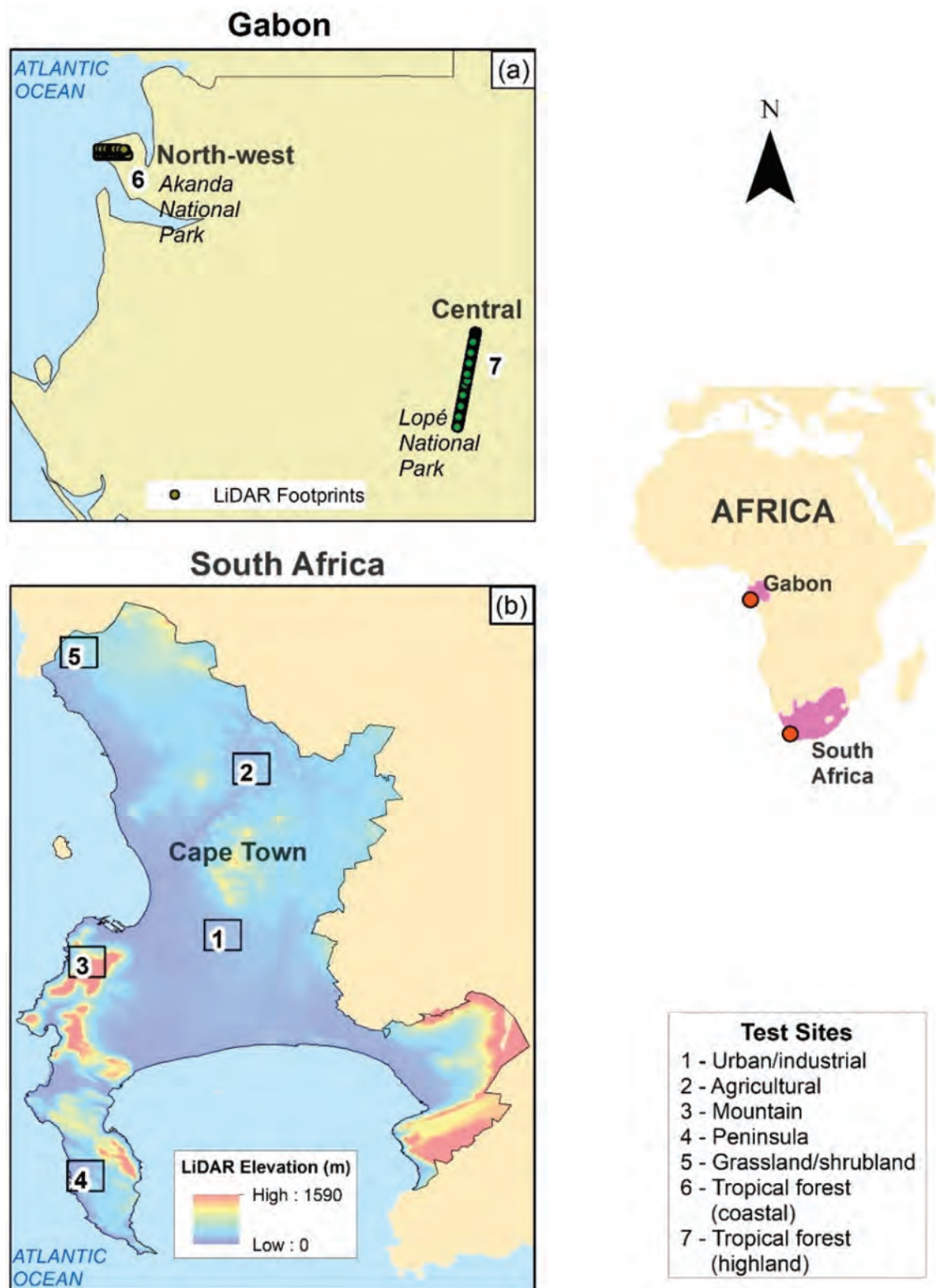


**Figure 2.** Maps showing the selected test sites for the vertical accuracy assessment – (a) Akanda and Lopé National Parks in North-west and Central Gabon respectively (b) Cape Town, located in the Western Cape Province of South Africa.

of Economy, Trade and Industry (METI) of Japan. ASTER GDEM was produced using imagery acquired from the NASA Terra mission (Altunel, Okolie, and Kurtipek 2022). The DEM was generated from stereo images of the ASTER optical sensor onboard the Terra satellite. ASTER GDEM version 1 was released at 1 arc-second postings in

2009. Improved versions of the GDEM were later released: version 2 in 2011 and version 3 in 2019.

### 2.2.3. Copernicus DEM (GLO-30)

Copernicus DEM was released in 2020, and is derived from the WorldDEM data. The WorldDEM data product is based on the radar satellite data which was

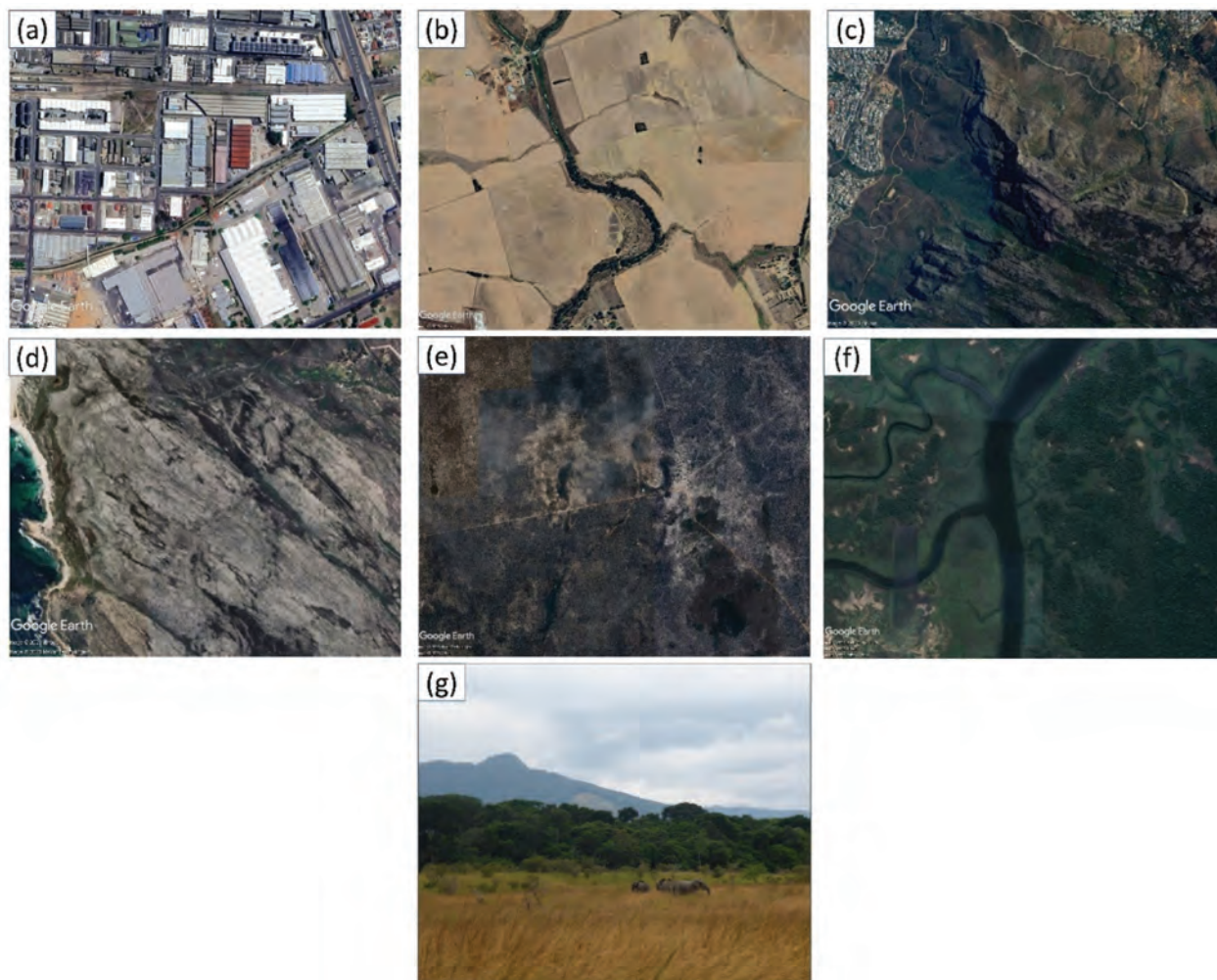


**Figure 3.** Pictorial views of the different landscapes considered – (a) Urban/Industrial (b) Agricultural (c) Mountain (d) Peninsula (e) Grassland/shrubland (f) Tropical rainforest, coastal (g) Tropical rainforest, highland. Sources: author's compilation; Google Earth; Ngangorica (2014).

**Table 1.** General characteristics and description of landscapes assessed in this study.

Test area	Landscape	Description
Cape Town, South Africa	Whole area	Mixture of landscapes.
	Urban/Industrial	Densely built-up residential, commercial and industrial areas in Cape Town Municipality.
	Agricultural land	Cultivated fields and few farm settlements. Meeting point of the Diep River and Mosselbank River.
	Grassland/shrubland/dense bush	Light vegetation, shrubs, open grassland and dense bushes, southeast of Grotto Bay.
Cape Peninsula	Mountainous	Flat-topped Table Mountain National Park, with the adjoining Camps Bay and Happy Valley.
	Peninsula	Low-lying and gently sloping section of the Cape Peninsula, in the general vicinity of Olifantsbos Beach, Miller's Point and Partridge Point. Plant formations in the Cape Peninsula include shrublands, grasslands, forest and thicket.
Akanda and Lopé National Parks, Gabon	Whole area	Mixture of forests.
	Akanda National Park (Tropical rainforest, coastal)	Mangrove forests and tidal beaches of Akanda National Park, along the bay of Mondah.
	Lopé National Park (Tropical rainforest, highland)	Dense gallery forest of the Lopé National Park in the Central highlands of Gabon. River Ogooué runs through the north of Lopé.

acquired during the TanDEM-X mission (Airbus 2020a). The primary objective of the TanDEM-X mission was the generation of a global coverage DEM based on InSAR in HRTI-3 standards. The duration of the TanDEM-X data acquisition was between December 2010 and January 2015. The Copernicus GLO-30 dataset has a grid spacing of 1 arc-second

(30 m) and is available at a standardized extent of  $1^\circ \times 1^\circ$ . The DEM is available in two different formats, DGED and DTED. For this study, the floating point DGED format was adopted. The Copernicus DEM has been assessed with ICESat-2 measurements, which indicate absolute vertical uncertainties of  $\sim 1\text{--}3$  m (Airbus 2020a, 2020b).

**Table 2.** Characteristics of the datasets used.

Dataset	Sensor (Source)	Coverage	Horizontal datum	Vertical datum	Height system	Precision	Data acquisition period	Release date of most recent version
NASADEM	C-band radar (NASA)	56°S – 60°N	WGS84	EGM96	Orthometric	Integer	2000	2020
ASTER GDEM	Optical/stereo NIR imagery (NASA/JAXA)	83°S – 83°N	WGS84	EGM96	Orthometric	Integer	2000–2013	2019
Copernicus GLO-30	X band radar (ESA/Airbus)	Entire Earth	WGS84	EGM2008	Orthometric	Floating point	2010–2015	2021
ALOS World 3D	Optical/stereo pan imagery (JAXA)	82°S – 82°N	WGS84	EGM96	Orthometric	Integer	2006–2011	2022
City of Cape Town (CCT) aerial LiDAR	Information and Knowledge Management Division, City of Cape Town	Cape Town Municipality	Hartebeesthoek94	SAGEOID10 (Land Levelling Datum, LLD)	Orthometric	Floating point	2018–2021	–
LVIS AfriSAR	NASA Land Vegetation and Ice Sensor	AfriSAR coverage area, Gabon	WGS84	WGS84	Ellipsoidal	Floating point	2016	–

Sources: Author's compilation; Takaku et al. (2015), Guth and Geoffroy (2021), Hawker et al. (2019), Purinton and Bookhagen (2021), and Airbus (2020a, 2020b)

**Table 3.** Tile IDs of datasets used in this study.

Dataset	Cape Town	Akanda and Lopé National Parks
NASADEM	s34e018 s35e018	n00e009 s01e011 s02e011
ASTER	ASTGTMV003_S34E018 ASTGTMV003_S35E018	ASTGTMV003_N00E009 ASTGTMV003_S01E011 ASTGTMV003_S02E011
Copernicus	Copernicus_DSM_10_S34_00_E018 Copernicus_DSM_10_S35_00_E018	Copernicus_DSM_10_N00_00_E009 Copernicus_DSM_10_S01_00_E011 Copernicus_DSM_10_S02_00_E011
AW3D	ALPSMLC30_S034E018 ALPSMLC30_S035E018	ALPSMLC30_N000E009 ALPSMLC30_S001E011 ALPSMLC30_S002E011
AfriSAR LVIS	–	LVIS2_Gabon2016_0308_R1808_045612 LVIS2_Gabon2016_0222_R1808_044757

#### 2.2.4. ALOS World 3D DEM v3.2

In 2016, the Japan Aerospace Exploration Agency (JAXA) released the 30 m Advanced Land Observing Satellite World 3D (ALOS World 3D – AW3D30) DEM. AW3D30 was generated from the earlier ALOS DEM which was produced at a spatial resolution of 5 m with an accuracy of 5 m (standard deviation) (JAXA 2023). AW3D30 has undergone several developmental phases including void filling and reduction in absolute offsets (JAXA 2019; Okolie and Arungwa 2022). The most recently available version 3.2 was adopted in this study.

#### 2.2.5. City of Cape Town airborne LiDAR DEM

The City of Cape Town (CCT) airborne LiDAR DEM was acquired from the Information and Knowledge Management Department of the City of Cape Town (CCT 2023). The 2 m DEM is generated from the LiDAR point cloud, at a maintenance cycle of 3 years. For data acquired prior to 2021, the point density is 2–3 points/m<sup>2</sup>, but this has been upgraded to 10 points/m<sup>2</sup> post-2021. The height accuracy of the point cloud is 0.15 m. The data acquisition for

the dataset used in this study was conducted in phases between 2018 and 2021. The gridded format is derived through the processing of the ground-classified LiDAR point clouds using triangulation in LP360, an advanced desktop LiDAR software package (LP360 2022). The DEM is spatially referenced to the Hartebeesthoek94 horizontal coordinate system. The height reference used is South Africa Land Levelling Datum (SAGEOID2010) (Chandler and Merry 2010).

#### 2.2.6. AfriSAR LVIS L2 geolocated surface elevation products

The Land Vegetation and Ice Sensor is an airborne, medium-altitude scanning laser altimeter designed and developed by the Laser Remote Sensing Laboratory at NASA's Goddard Space Flight Centre to measure sub-canopy ground elevation, vegetation structure and topography of ice sheets and glaciers (Blair, Rabine, and Hofton 1999; Fatoyinbo et al. 2021; Sun et al. 2008). Between February – March 2016, LVIS was flown over selected sites in Gabon, Africa, as part of the AfriSAR Campaign



(Fatoyinbo et al. 2021; NASA 2020). The goal of the campaign was to collect ground, airborne SAR and airborne LiDAR data for the development and evaluation of forest structure and biomass retrieval algorithms (Fatoyinbo et al. 2017). AfriSAR provided overlapping along track footprints with a nominal footprint diameter of 22 m with 9 m separations (Blair and Hofton 2018; Blair, Rabine, and Hofton 1999; Fatoyinbo et al. 2021). For this study, the Level 2 Geolocated Surface Elevation Product, version 1 (Blair and Hofton 2018) which contains the canopy top and ground elevations were downloaded in ASCII format from the archive of the National Snow and Ice Data Centre (NSIDC). The vertical datum of the AfriSAR data is the WGS84 ellipsoid.

### 2.3. Harmonisation of datums and spatial reference systems

#### 2.3.1. Horizontal datum transformation

The global DEMs and AfriSAR LVIS data were all transformed from the geographic to the Universal Transverse Mercator (UTM) projection in WGS84. Similarly, the Cape Town LiDAR DEM was transformed from Hartebeesthoek94 to UTM WGS84. The transformations were carried out using the projection tool within ArcGIS software. It is generally understood that map projections incur some level of distortion during the process of transforming 3D spherical coordinates onto a plane (Laurini and Thompson 1992). However, UTM minimizes projection distortions and is recommended for areas between latitudes 84°N to 80° S (Emery and Camps 2017; Jain and Singh 2003).

#### 2.3.2. Vertical datum transformation

The vertical datum of the AfriSAR data is WGS84 (i.e. the data are referenced horizontally and vertically to the WGS84 ellipsoidal, global reference system) (Hofton et al. 2006, 2002; Ni, Sun, and Ranson 2013, 2014a, 2014b). Consequently, the LVIS data were converted to orthometric heights, with respect to the EGM2008 geoid. The difference between the ellipsoidal height ( $h$ ) and the geoid height/undulation ( $N$ ) gives the orthometric height ( $H$ ), that is:

$$H = h - N \quad (1)$$

There are significant differences between EGM96 and EGM2008 vertical datums. The development of EGM2008 followed a more rigorous approach and better algorithms that resulted in a more accurate model (Roman, Wang, and Saleh 2010). Compared to EGM96, EGM2008 offers a significant improvement in the estimation of topographical heights (Pavlis et al. 2012; Üstün, Abbak, and Öztürk 2016). In a numerical investigation in Turkey, Üstün et al. (2016) showed that a possible transformation from EGM96 to EGM2008 could yield more accurate heights with an improvement

of up to 2.5 m. In external validations of EGM2008 over parts of Africa, e.g. South Africa (Merry 2009) and Algeria (Benahmed Daho 2009) it provided a better agreement than EGM96 when compared to Global Positioning System (GPS)/leveling data. The review of previous studies favors the adoption of EGM2008 as a common vertical datum for the DEMs in this study. Moreover, the use of EGM2008 in topographic mapping projects has been encouraged (e.g. Rao et al. 2012).

The EGM96 and EGM2008 geoid models were downloaded from the website of the International Centre for Global Earth Models (Sinem Ince et al. 2019). The parameters defined for retrieving the geoid models through ICGEM online are shown in Supplementary Table S1. The geoid heights were downloaded in plain text format at a grid spacing of 0.0005°. The grids were converted to raster surfaces through Inverse Distance Weighted (IDW) interpolation in ArcGIS 10.8 (shown in Supplementary Figures S1–S4), and the differences in the geoid heights were calculated. Thereafter, the vertical datum conversion from EGM96 to EGM2008 was carried out within the ArcGIS raster calculator, using the equation by Üstün et al. (2016).

$$\begin{aligned} H_{EGM08} &= H_{EGM96} + N_{EGM96} - N_{EGM08} \\ &= H_{EGM96} + \delta N \end{aligned} \quad (2)$$

where,

$H_{EGM96}$  is the elevation of DEM based on EGM96 model.

$H_{EGM08}$  is the elevation of DEM based on EGM2008 model.

$N_{EGM96}$  is the geoid height based on EGM96 model.

$N_{EGM08}$  is the geoid height based on EGM2008 model.

$\delta N$  is the geoid height difference between EGM96 and EGM2008.

It was also required to transform the CCT LiDAR DEM to EGM2008. The SAGEOID10 geoid model was acquired from the national mapping agency of South Africa (Chief Directorate: National Geo-spatial Information). The data is in the form of an ASCII data file, on a 2.5' grid compatible with EGM2008 data. The SAGEOID10 and EGM2008 grids were interpolated to raster surfaces with the same cell size as the LiDAR DEM. Thereafter, the vertical datum conversion to EGM2008 was conducted.

$$\begin{aligned} H_{EGM08} &= H_{SAGEOID10} + N_{SAGEOID10} - N_{EGM08} \\ &= H_{SAGEOID10} + \delta N \end{aligned} \quad (3)$$

where,

$H_{SAGEOID10}$  is the elevation of LiDAR DEM based on SAGEOID10 model.

$H_{EGM08}$  is the elevation of LiDAR DEM based on EGM2008 model.

$N_{SAGEOID10}$  is the geoid height based on SAGEOID10 model.



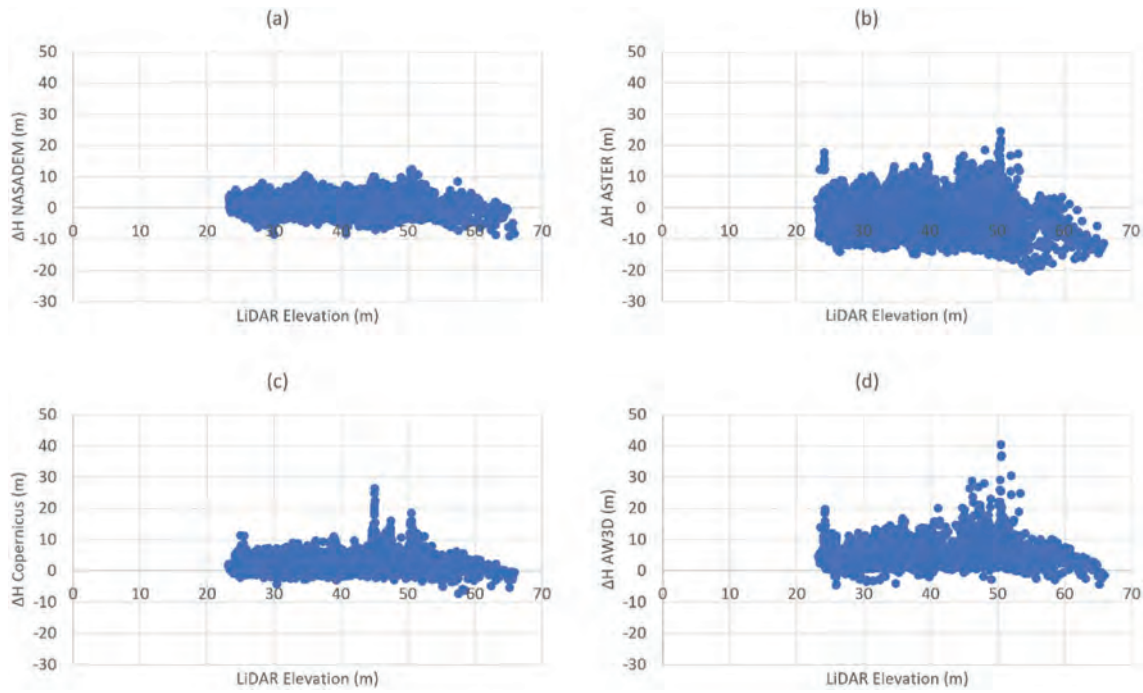


**Figure 4.** Graphical representation of the variations in elevation error, extracted from the raw data before three-sigma outlier filtering – urban/industrial landscape.

$N_{EGM08}$  is the geoid height based on EGM2008 model.

$\delta N$  is the geoid height difference between SAGEOID10 and EGM08.

#### 2.4. Data preparation

To obtain reliable accuracy measures, the sample size (number of checkpoints) should be sufficiently large. Two separate grids of points were created, 2,760,581 data points for Cape Town and 709,868 data points for Gabon. Using the “extract multi values to points” tool in ArcGIS, the corresponding elevations from LiDAR, NASADEM, ASTER, Copernicus and AW3D that intersected the points were extracted and recorded within the attribute tables of the data points.

#### 2.5. Outlier filtering and screening of water pixels

The elevation errors ( $\Delta H$ ) were calculated by subtracting the LiDAR elevations from the corresponding elevations of each global DEM. This was followed by cleaning and outlier filtering carried out in three stages. In the first stage, all DEMs were checked and negative elevation values were removed (this is advisable because of inconsistencies in water body flattening among global DEMs). After this first stage of cleaning, we applied the Three-sigma rule (Wessel et al. 2018) for outlier filtering. Values outside the mean height difference ( $\Delta h_{mean}$ ) plus/minus three times the standard deviation ( $\Delta h > \Delta h_{mean} + 3 * SD$ ,  $\Delta h < \Delta h_{mean} - 3 * SD$ ) were eliminated. The third

stage involved the removal of elevation points occurring on water bodies. There is some uncertainty regarding the accuracy of DEMs over water bodies. Moreover, specular reflection and temporal decorrelation in interferometric SAR acquisition and processing could cause smooth water bodies to appear as rough surfaces in InSAR DEMs (Ettritch et al. 2018; Huber et al. 2021). Consequently, elevation points within the boundaries of natural and artificial water bodies, including dams in Cape Town (identified from Google Earth imagery and the Cape Town waterbodies dataset) were removed. This resulted in a final set of 2,570,126 (Cape Town) and 625,647 (Gabon) points for validation of the DEMs.

#### 2.6. Accuracy assessment

Qualitative (visual) and quantitative analysis are among the standard and advanced checks described in Gesch et al. (2014) and Cenci et al. (2021) as quality assessment criteria for DEMs. Visual analysis is a basic and powerful approach that can quickly reveal the existence of problems in DEMs (Mesa-Mingorance and Ariza-López 2020). The absolute vertical accuracy is assessed by calculating the difference between the satellite DEMs and the reference DEM (LiDAR) (Cenci et al. 2021). The elevation values from the airborne LiDAR and satellite DEMs were extracted wherever they intersected with points in the grid. This analysis of the elevation difference ( $\Delta H$ ) enables the detection of possible random errors and systematic bias (Cenci et al. 2021).

The elevation errors or differences ( $\Delta H$ ) between the DEMs and reference LiDAR were calculated as follows:

$$\Delta H = H_{GlobalDEM} - H_{RefDEM} \quad (4)$$

where,

$H_{RefDEM}$  = elevation from LiDAR.

$H_{GlobalDEM}$  = individual elevations from NASADEM, ASTER, Copernicus and AW3D.

Correlation analysis enabled the analysis of the inter-relationships between the elevation errors. Using the statistical populations of the  $\Delta H$  and/or  $|\Delta H|$ , several accuracy metrics were computed as follows: Mean Error (ME), Standard Deviation (SD), Root Mean Square Error, Mean Absolute Error (MAE), Median Absolute Deviation (MAD), Normalised Median Absolute Deviation (NMAD), and Linear Error at 95% (LE95) confidence level respectively. The ME indicates the presence of bias in the data, the MAE represents the average magnitude of the elevation errors, but without considering their direction, while the RMSE penalizes large errors (Carrera-Hernández 2021). However, the RMSE also has limitations as an accuracy measure. For example, it does not distinguish between random errors, systematic errors or blunders; and the errors in a DEM do not always follow a normal distribution (Carrera-Hernández 2021; Höhle and Höhle 2009; Wise 2000). The MAD and NMAD overcome these limitations due to their robustness and distribution free approach to handling data outliers (Carrera-Hernández 2021; Höhle and Höhle 2009; Willmott and Matsuura 2005).

The equations are given as follows:

$$ME = \frac{\sum_{i=1}^n (\Delta H)}{n} \quad (5)$$

$$MAE = \frac{\sum_{i=1}^n (|\Delta H|)}{n} \quad (6)$$

$$SD = \sqrt{\sum_{i=1}^n \frac{(\Delta H_i - \underline{\Delta H})^2}{n-1}} \quad (7)$$

$$RMSE = \sqrt{\frac{1}{n} \sum_{i=1}^n (\Delta H_i)^2} \quad (8)$$

where,

$\underline{\Delta H}$  = mean of the height differences.

The MAD and NMAD were calculated as follows. (Höhle and Höhle 2009; Wessel et al. 2018):

$$MAD = MD(|(\Delta H_i - MD_{\Delta H_i})|) \quad (9)$$

$$NMAD = 1.4826 \times MAD \quad (10)$$

The NMAD is more resilient to outliers in the dataset (Höhle and Höhle 2009). At confidence level of 95%, the LE is calculated as given below:

$$LE95 = SD \times 1.96 \quad (11)$$

In the above equations,  $n$  is the number of points under consideration,  $MD$  represents the median of a set of elevation data, while  $MD_{\Delta H_i}$  represents the median of the elevation differences or the 50% quartile (Grohmann 2018). The descriptive statistics were summarized using SPSS (IBM 2023) and Microsoft Excel (Microsoft 2023), while statistical visualizations were generated with R (R Project 2022) software.

### 2.6.1. Height error maps

Height Error Maps (HEMs) were generated by subtracting the LiDAR DEM from the global DEMs, as a visual estimation of the height error in different landscapes (Gdulová, Marešová, and Moudrý 2020). According to Hawker et al. (2019), such maps are useful for visualizing the spatial distribution of elevation errors and enable an indication of the error sources.

### 2.6.2. Error ranking

Using the calculated accuracy measures, we computed the relative ranks of the DEMs to gain a better understanding of their performance. The ranking method adopted in this study was proposed by Poudel and Cao (2013) and defined as follows:

$$R_i = 1 + \frac{(m-1)(S_i - S_{min})}{(S_{max} - S_{min})} \quad (12)$$

where  $R_i$  is the relative rank of the DEMs ( $i=1, 2, \dots, m$ ),  $S_i$  is the basis of error values produced by each DEM,  $S_{min}$  is the minimum value of  $S_i$ ,  $S_{max}$  is the maximum value  $S_i$ , and  $m$  is the number of DEMs. With this ranking system, the most accurate and the least accurate DEMs have relative ranks of 1 and  $m$ , respectively, while the ranks of the other DEMs are expressed as real numbers between 1 and  $m$ . This ranking approach has already been adopted in similar studies (e.g. Altunel, Okolie, and Kurtipek 2022).

### 2.6.3. Influence of tree cover on vertical accuracy

Using the global tree cover dataset from the Global Land Analysis And Discovery (GLAD 2023), the variation in DEM accuracy based on percentage tree cover was assessed. The global tree cover data (treecover2010) provides estimates of circa 2010 % maximum (peak of growing season) tree canopy cover derived from Landsat 7 ETM+ imagery. It represents the estimated maximum tree canopy cover (1–100% for the year 2010 in integer values ranging from 1–100) (GLAD 2023). In the Landsat analysis for treecover2010 which was carried out in Earth Engine, trees were defined as all vegetation taller than 5 m, and the methodology is extensively discussed in Hansen et al. (2013).

### 2.6.4. Relationship with slope and aspect

The next analysis involved an assessment of the relationship between vertical error and two primary topographic parameters, slope and aspect. These parameters often display noticeable uncertainties due to the vertical errors in DEMs. The vertical error of DEMs and their derived parameters are of great importance since the vertical errors can be propagated to the parameters (e.g. Altunel2021; Nwilo et al. 2022). The slope and aspect maps were generated from LiDAR using QGIS software. Subsequently, the elevation errors from the global DEMs were categorized into different slope and aspect classes for further analysis.

## 3. Results and discussion

### 3.1. Height error distribution and analysis

Table 4 shows the range of values (minimum and maximum) and mean elevations of the DEMs. In Cape Town, the elevation ranges from 0 to 1590 m, while the mean elevation ranges from 116–124 m with the lowest mean occurring in ASTER GDEM. Some of the highest points in Cape Town are in the eastern

suburbs around the Lourensford dam, on the Table Mountain and on Chapmans Peak. In densely forested Gabon, the elevation ranges from 0–846 m, while the mean elevation ranges from 330–354 m.

For a preliminary exploration, Figures 4–10 show graphical representations of the elevation error, before applying the Three-sigma rule for outlier filtering. Within the urban/industrial area (Figure 4), most errors occur within an elevation range of 23–60 m. Although buildings are known to inhibit the penetration of radar signals on land surfaces (Olajubu et al. 2021), Copernicus DEM shows the least error dispersion in this urban area, unlike ASTER and AW3D. Similarly, in the agricultural lands (Figure 5), the errors in ASTER and AW3D are more widely dispersed, whereas the two SAR DEMs (NASADEM and Copernicus) display a narrower error dispersion. As the elevation increases, the number of height points decrease. According to Hoja et al. (2006), the quality of a DEM derived from one source is influenced by land cover type and the steepness of the terrain. The Table Mountain slopes downward into the adjoining Camps Bay, and this might explain the gradual increase in the height errors between 0–400 m, where the error range is approximately between –50 to 50 m, and the progressive

Table 4. Summary of the elevation ranges.

DEM	Cape Town, South Africa			Akanda and Lopé National Parks, Gabon		
	Min (m)	Max (m)	Mean (m)	Min (m)	Max (m)	Mean (m)
LiDAR 2 m	0.00	1589.18	120.60	0.02	834.98	329.86
NASADEM 30 m	0.00	1590.51	121.46	0.97	828.21	347.91
ASTER 30 m	0.00	1578.51	116.04	1.92	837.21	347.26
Copernicus 30 m	0.00	1586.96	121.42	0.00	846.14	353.05
AW3D 30 m	0.00	1586.51	123.52	0.92	839.21	353.82

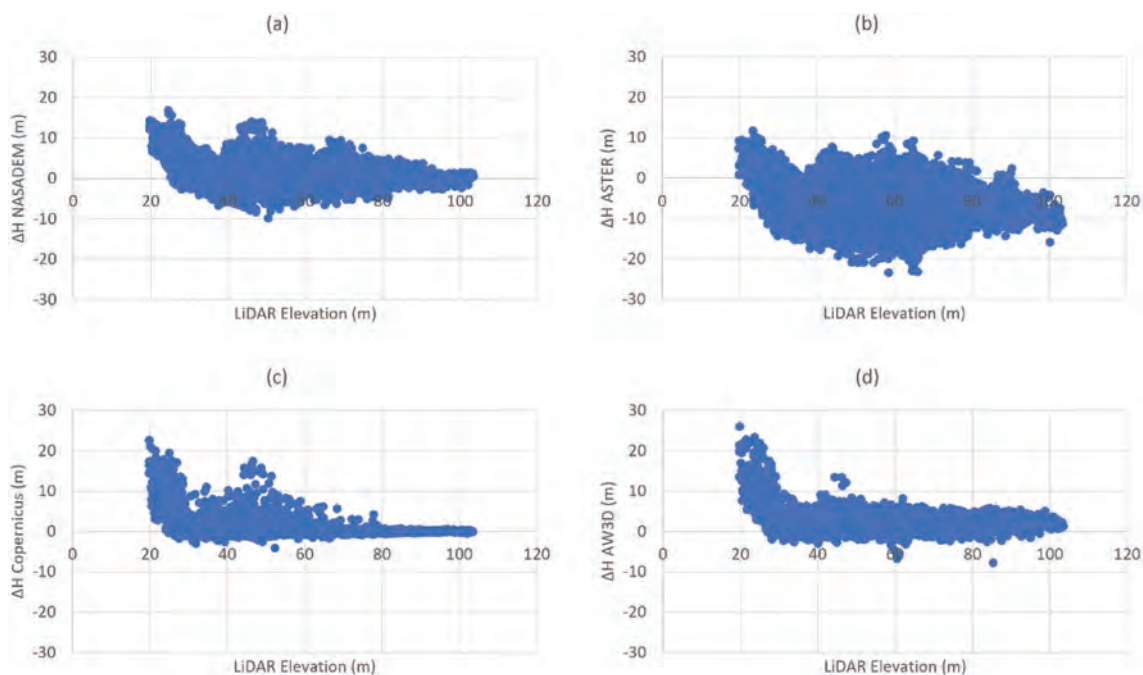


Figure 5. Graphical representation of the variations in elevation error, extracted from the raw data before three-sigma outlier filtering – agricultural land.



error escalation at higher altitudes (Figure 6). The highest positive offsets in the mountainous area occur in NASADEM and ASTER, while the highest negative offset is by Copernicus DEM. Generally, the errors range from  $-185$  to  $230$  m in the mountainous area.

The elevation error distribution after outlier filtering is visualized with histograms of the sampled errors in Figure 11 (Cape Town) and Figure 12 (Akanda and Lopé). These histograms are superimposed with curves for the normal distribution. Because outliers were

filtered from the data, the estimated curves are expected to match better with the data. Elevation errors that are positive indicate that the global DEMs overestimate the surface elevation while negative errors indicate areas where the surface elevation was underestimated. For Cape Town, there is a greater range of errors in the ASTER GDEM ( $-53.9$  m to  $18.6$  m; Figure 11(b)). A narrower spread of errors is observed in Copernicus ( $-12.20$  m to  $14.70$  m; Figure 11(c)) and AW3D ( $-9.6$  m to  $15.6$  m; Figure 11(d)).

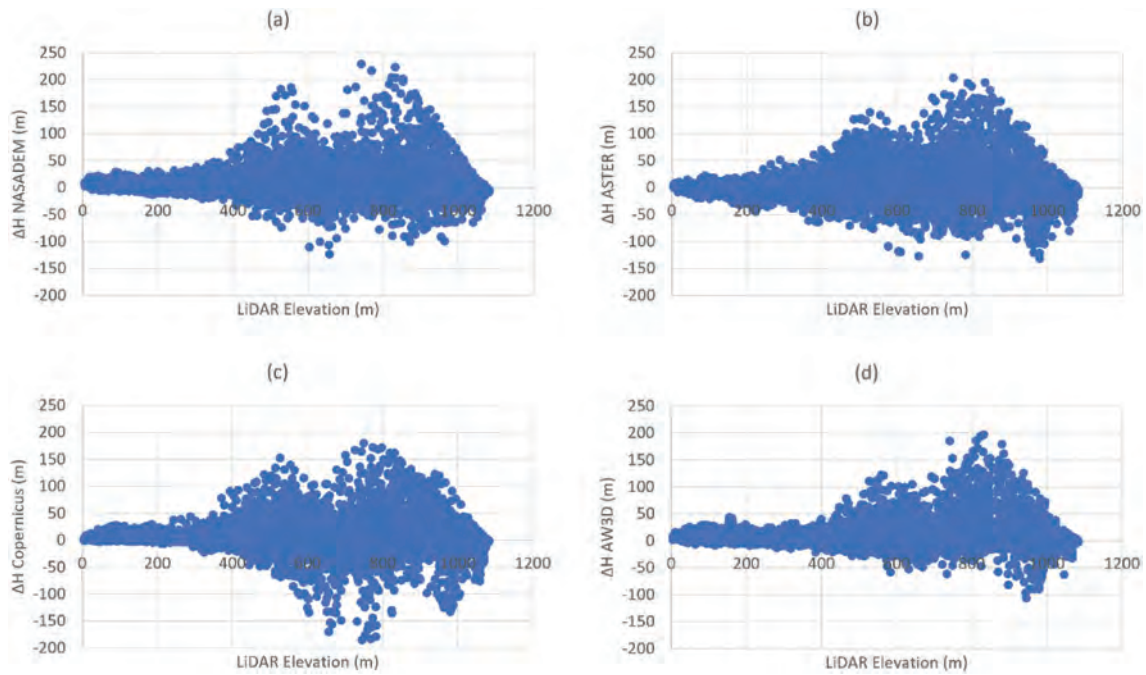


Figure 6. Graphical representation of the variations in elevation error, extracted from the raw data before three-sigma outlier filtering – mountain.

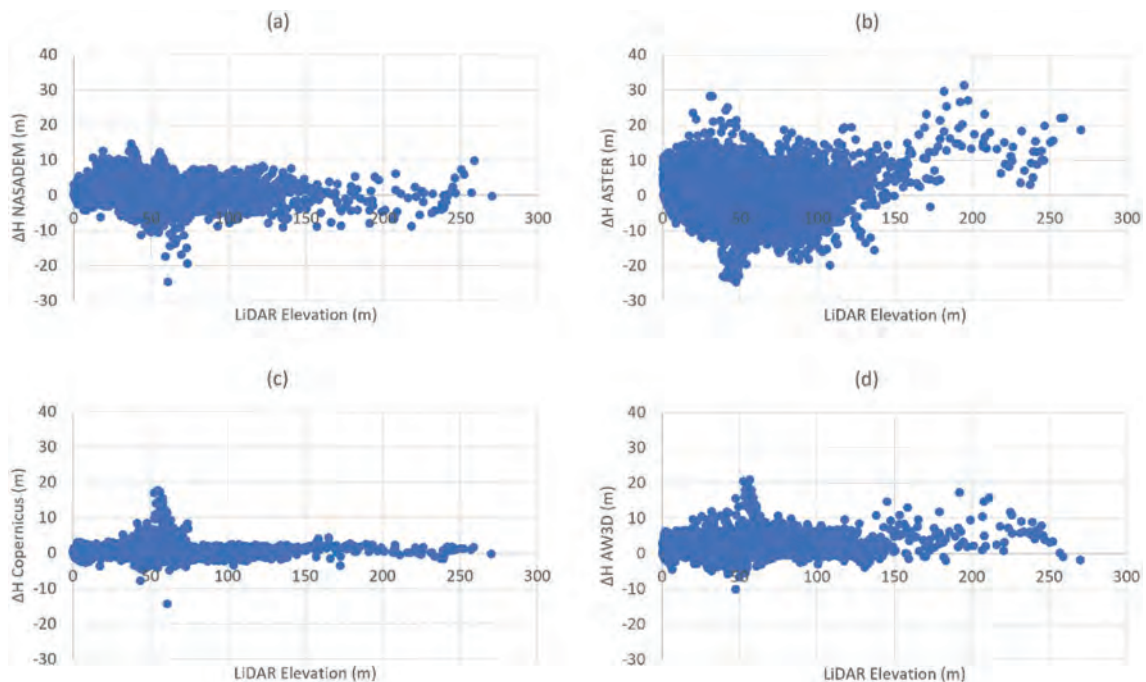
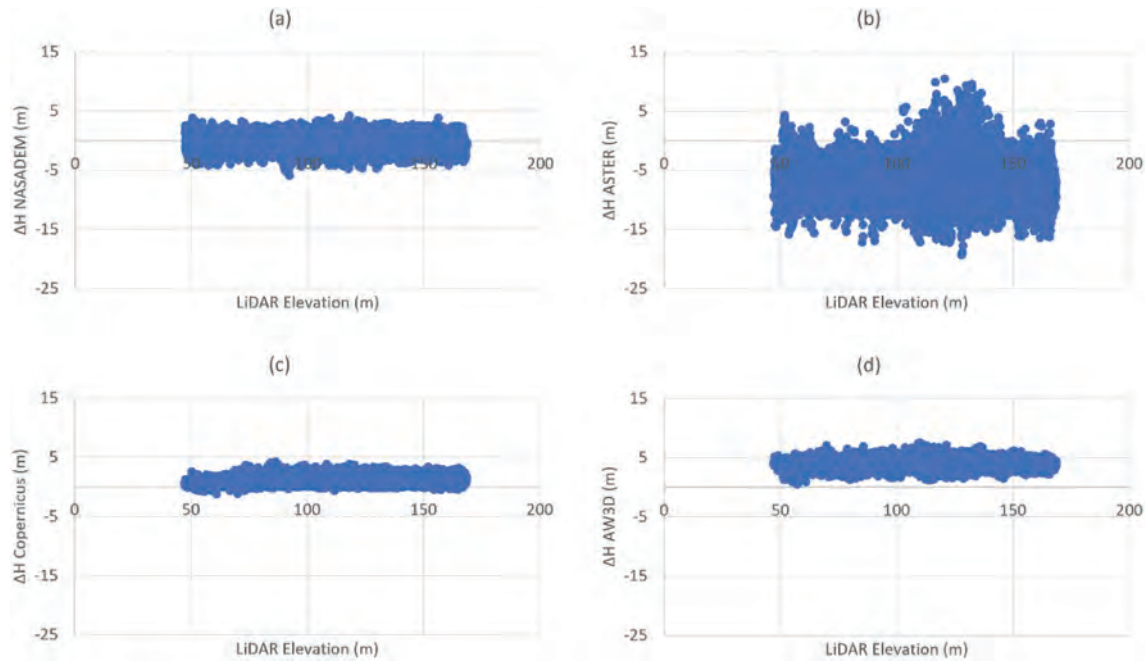
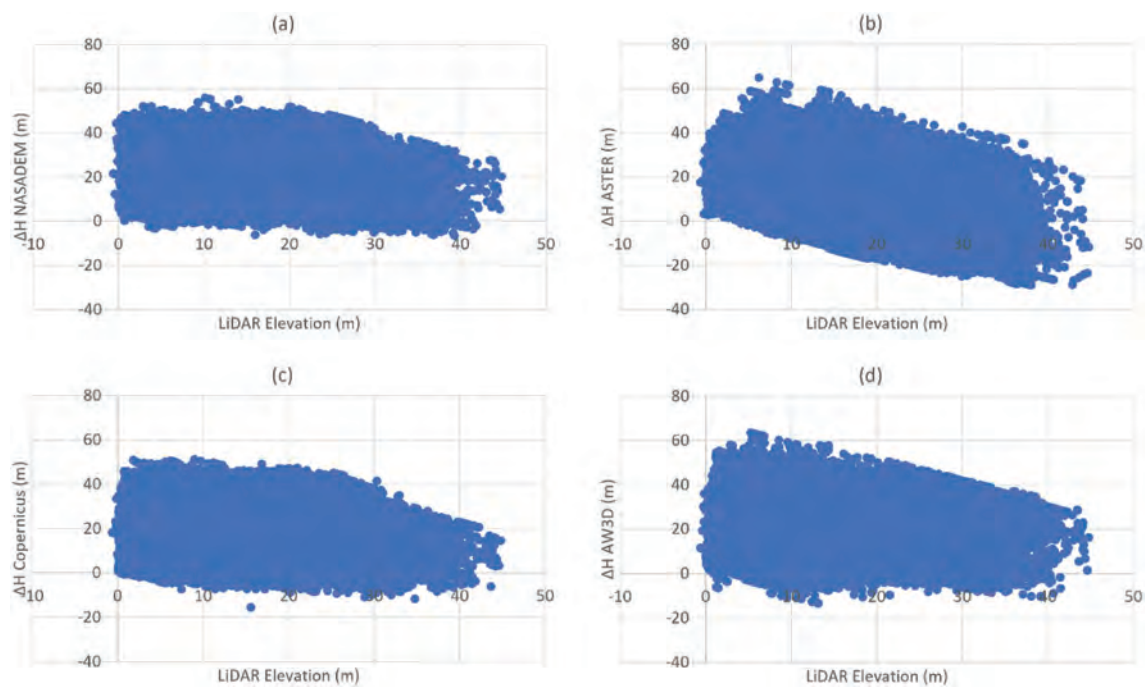


Figure 7. Graphical representation of the variations in elevation error, extracted from the raw data before three-sigma outlier filtering – peninsula.



**Figure 8.** Graphical representation of the variations in elevation error, extracted from the raw data before three-sigma outlier filtering – grassland/shrublands.



**Figure 9.** Graphical representation of the variations in elevation error, extracted from the raw data before three-sigma outlier filtering – tropical rainforest (coastal).

For better diagnosis of the distribution, quantile-quantile (Q-Q) plots for the same data distribution of  $\Delta H$  in Cape Town and Gabon are shown in Supplementary Figures S5 and S6 respectively. Generally, the Q-Q plots show some agreement with a normal distribution. However, in Cape Town, there is some moderate skewness and this is characteristic of the varied landscape consisting of natural and man-made features. For example, buildings, paved surfaces and artificial lakes could alter the random pattern of height errors on the

landscape. The Q-Q plots for  $\Delta H$  in Gabon indicate a closer alignment with normality. The natural forest landscape has spatial patterns and vertical structures that may not have been significantly altered by human activities.

### 3.2 Visual and qualitative analysis

Figures 13 and 14 present a visualization of the DEMs in the urban/industrial and agricultural landscapes in

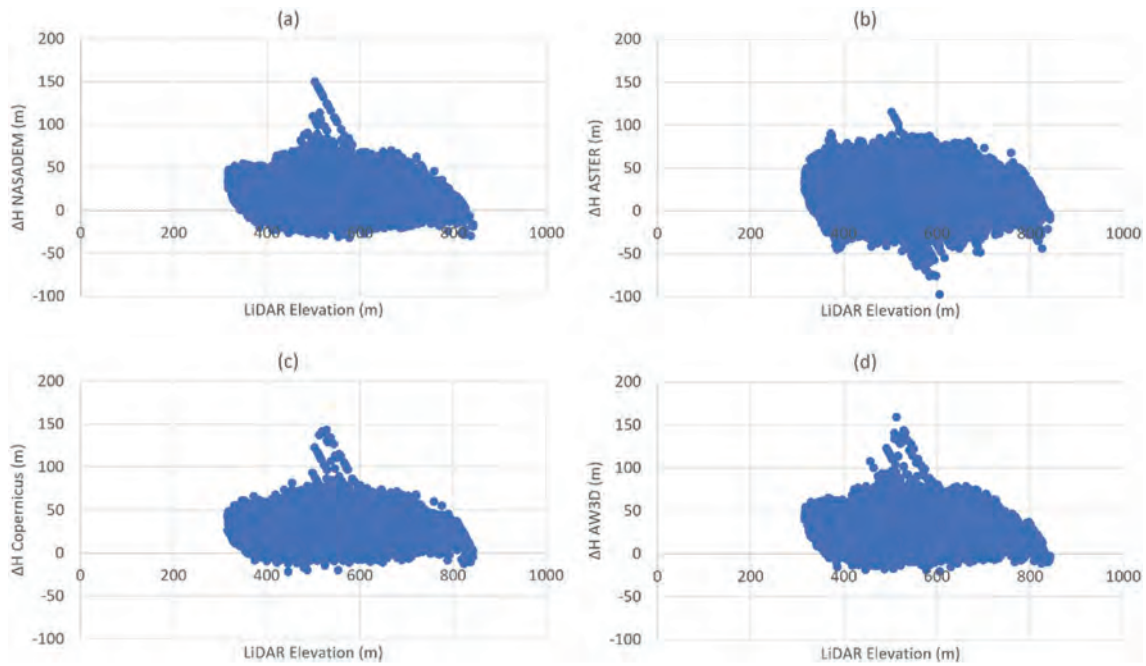


**Figure 10.** Graphical representation of the variations in elevation error, extracted from the raw data before three-sigma outlier filtering – tropical rainforest (highland).

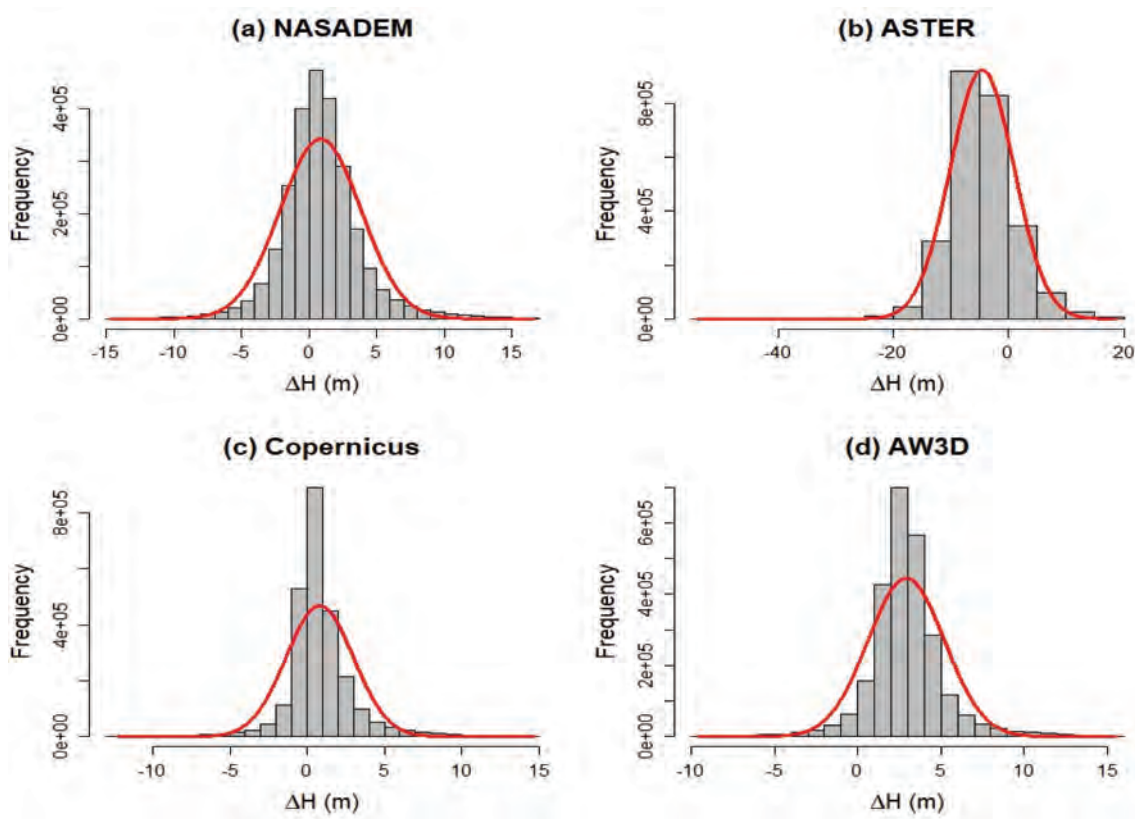


**Figure 11.** Histograms for the distribution of  $\Delta H$  in Cape Town, South Africa, (a) NASADEM (b) ASTER (c) Copernicus (d) AW3D, after outlier filtering.

Cape Town. This visual analysis enhances the understanding of differences in terrain characterization when using medium-resolution satellite-derived DEMs. The most detailed terrain representation and conditioning are achieved by LiDAR followed by Copernicus and AW3D. For example, in the

agricultural lands, the narrow channel of the Diep River and several tributaries are visible in both Copernicus (Figure 14(d)) and AW3D (Figure 14(e)), but poorly distinguishable in NASADEM (Figure 14(b)) and ASTER (Figure 14(c)). At 30 m pixel spacing, ASTER and NASADEM show a very



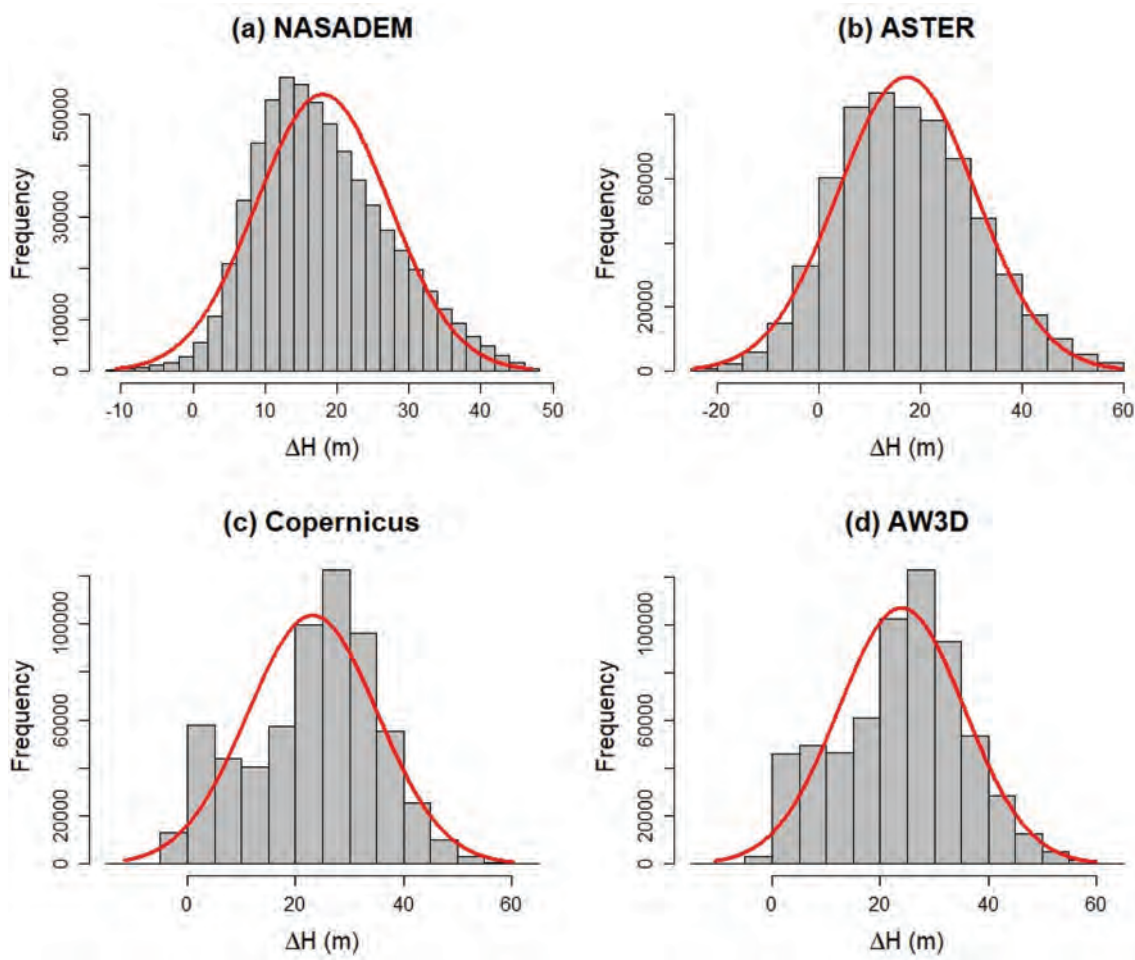


**Figure 12.** Histograms for the distribution of  $\Delta H$  in Akanda and Lopé National Parks, Gabon, (a) NASADEM (b) ASTER (c) Copernicus (d) AW3D, after outlier filtering.

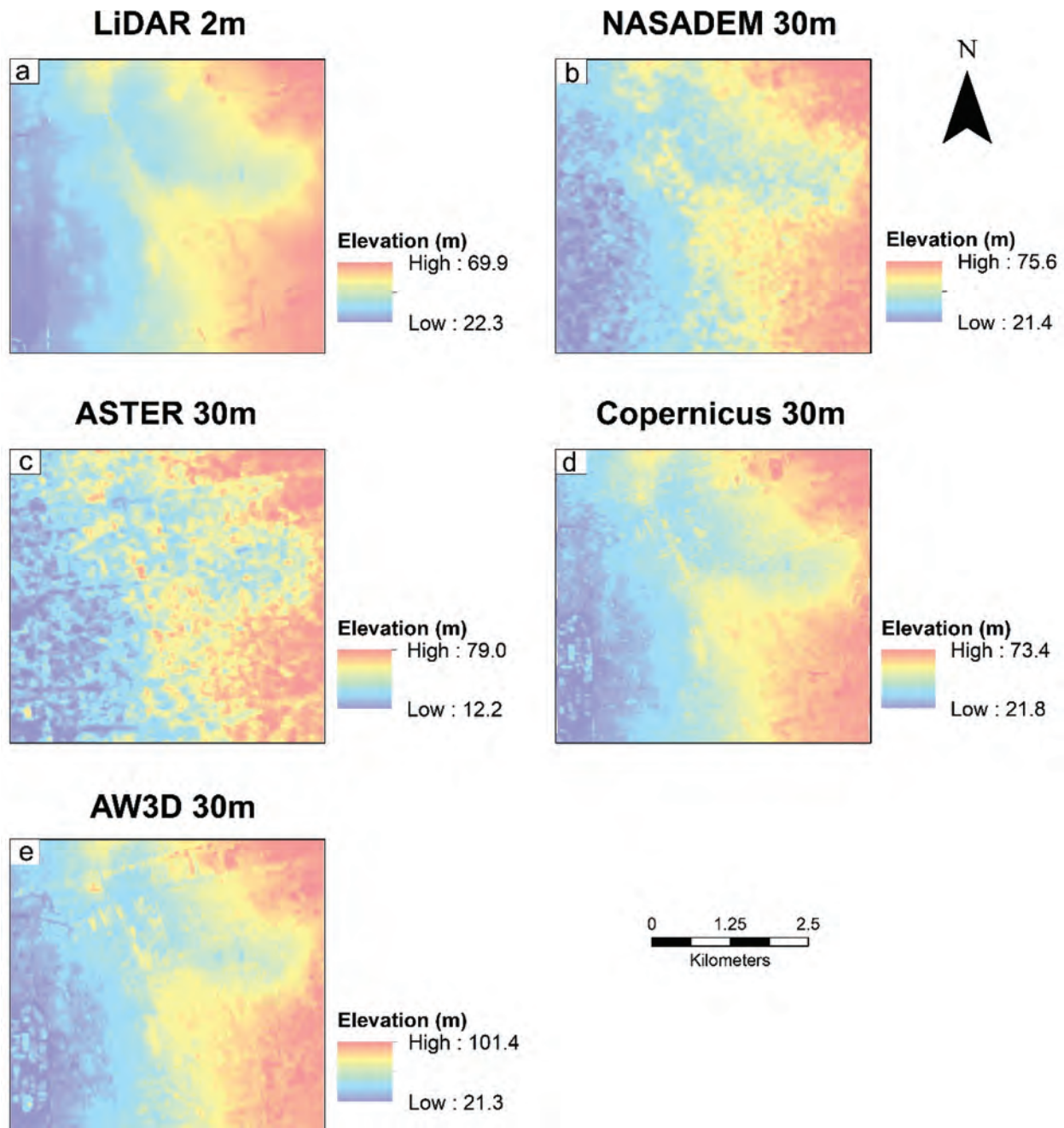
coarse surface characterization and terrain variability. Copernicus and AW3D show finer hydrological details in the agricultural lands (e.g. the narrow channel of River Diep is identifiable, and the dendritic drainage pattern is clearly discernible). The height variation in the urban/industrial area shows that moderate heights are associated with residential areas while the higher areas are associated with the industrial districts (e.g. Parow Industrial area). Building edges and outlines are better detected in Copernicus (Figure 13(d)) and AW3D (Figure 13(e)) but are diminished in NASADEM (Figure 13(b)) and ASTER (Figure 13(c)).

Figure 15 shows the height error maps (or DEMs of difference) generated for Copernicus DEM at sites in Cape Town. Positive offsets indicate areas where the elevation is overestimated by the DEMs and vice versa. The regions with the highest offsets are the urban center and industrial areas (Figure 15(a)), and the sloping edges of Table Mountain (Figure 15(c)) and Cape Peninsula (Figure 15(d)). Very high offsets are present along the slopes of the Table Mountain as seen in the saturated values (e.g. above 50 m). This pattern of increasing height errors in built-up areas and mountainous regions is not uncommon, and could be exacerbated by single or

double bounce scatter during SAR data acquisition (Nwilo et al. 2022; Schlaffer et al. 2015; Tsyganskaya et al. 2016). The problem of SAR measurements in steep slopes or mountains due to shadow, layover and foreshortening have also been well documented in the literature (e.g. Wessel et al. 2018). However, the flat top of the Table Mountain appears smoother and less affected by the SAR measurement errors. This is corroborated by Wessel et al. (2018). In their accuracy assessment of the global TanDEM-X DEM where the Table Mountain featured among the test sites, there were no height offsets on the flat-top level of the mountain.

These offsets are worse in ASTER and NASADEM, and lowest in Copernicus and AW3D. The errors are easily distinguished to show that the higher positive offsets occur in industrial areas while higher negative offsets occur in the residential areas. Similarly, in the agricultural lands, higher positive offsets occur along the Diep River channel while higher negative offsets occur elsewhere along the floodplains.

In Gabon, the presented LiDAR maps (Figure 16(a,j)) were interpolated at 30 m spacing from the LVIS LiDAR points using the IDW method. The penetrative ability of LiDAR in thick forests is evident in the elevation range of 0.5–32.8 m at the Akanda site, which is far below the



**Figure 13.** View of the LiDAR and global DEMs in the urban/industrial landscape.

satellite DEMs which are higher than 70 m in some areas. ASTER tends towards a higher negative bias in both forested areas (Figures 16(g,p)) as corroborated by the histograms of the height error (Figure 12(b)). In the site at Lopé, (Figures 16(j-r)), there is a central hilly region that is draped by forests.

### 3.3. Analysis of vertical accuracy

In the following analysis, positive elevation offsets (or differences) indicate points on the ground where the satellite DEMs overestimate the ground surface elevation, while negative elevation offsets indicate areas where the satellite DEMs underestimate the true ground surface elevation. Table 5

shows the accuracy measures and error ranking of the DEMs (the lower the overall rank, the better the DEM's performance and vice versa). In Cape Town, NASADEM, Copernicus and AW3D had positive mean errors, which indicates that majority of their elevation values are systematically higher than the ground surface. Conversely, ASTER had the highest negative mean error which indicates that most of the ASTER values underestimate the ground surface. ASTER elevation values were the least precise in Cape Town (SD: 5.55 m) and Gabon (SD: 13.59 m). This indicates that the elevation offsets in ASTER have a large variability and are the most highly dispersed, as corroborated in the histograms.

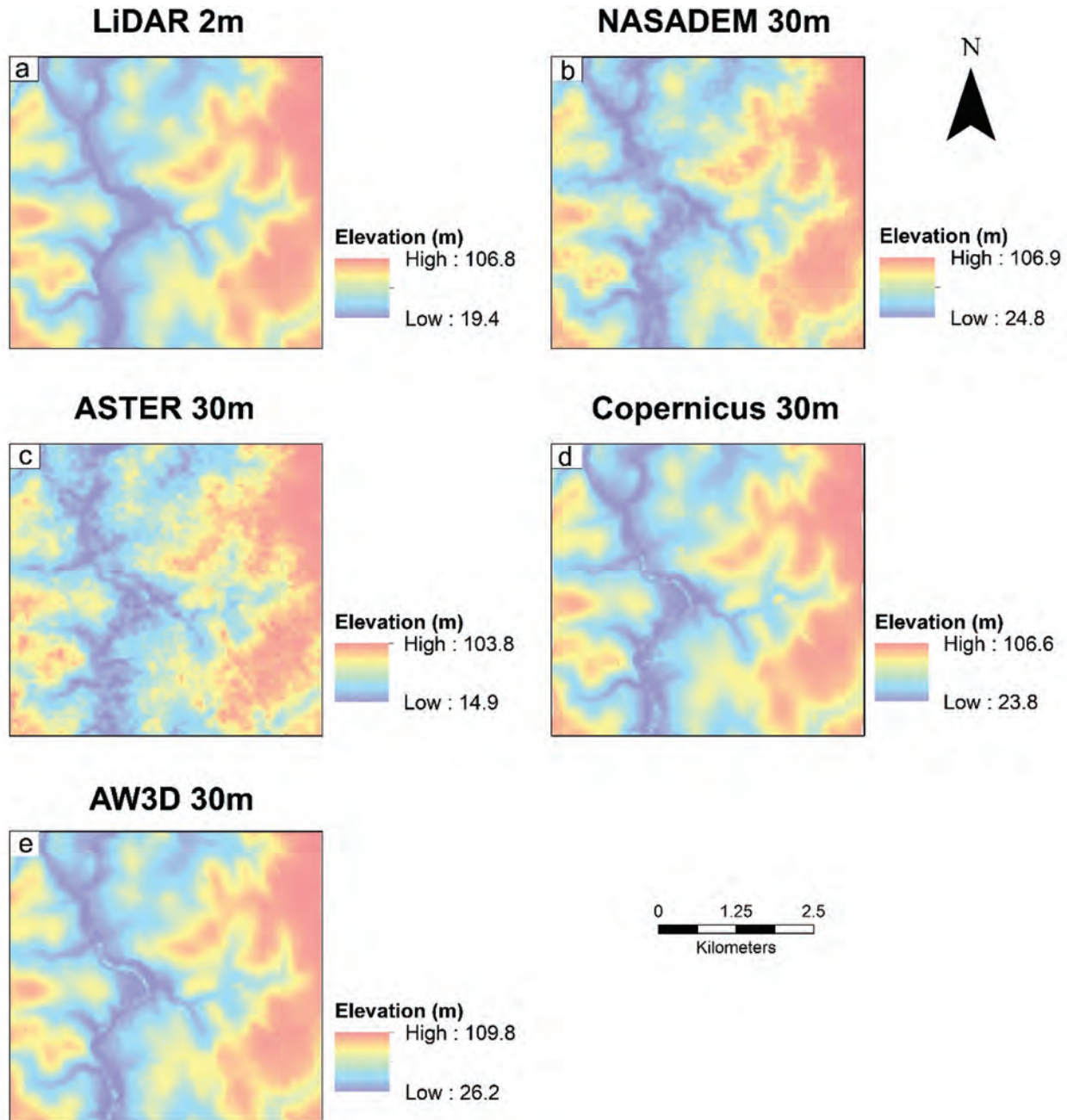


**Figure 14.** View of the LiDAR and global DEMs in the agricultural landscape.

AW3D and NASADEM had NMAD values of 1.47 m and 2.21 m respectively in Cape Town, occupying second and third place to Copernicus with an NMAD of 1.16 m. In Gabon, NASADEM and AW3D had the lowest NMAD values of 9.18 m and 11.15 m respectively, while Copernicus was placed third with an NMAD of 11.38 m.

In Cape Town, Copernicus DEM emerged as the most accurate DEM product, having the lowest mean error, SD, RMSE, MAE, NMAD, and linear error. Intermediately, NASADEM and AW3D occupied the second and third place but with no clear distinction between them. For example, NASADEM had a lower mean error, RMSE and MAE compared to AW3D. However, AW3D surpassed NASADEM with lower SD, NMAD and linear error. However, in terms

of the overall ranking, NASADEM is ranked higher than AW3D. The vertical accuracy of ASTER GDEM was the poorest in all the metric evaluations in Cape Town. In the overall ranking for Cape Town, Copernicus occupied first place and emerged as the most accurate DEM. NASADEM is ranked in second place followed by AW3D in third place, while ASTER GDEM has the lowest rank.

The trend is different in the dense forests of Gabon, which are spread over coastal plains and highlands. In both landscapes, all four DEMs show a notable tendency to overestimate the true ground surface, as evident in the high positive mean errors. AW3D had the highest mean error of 23.96 m while ASTER GDEM had the lowest mean error of 17.40 m. Generally, the elevation accuracy deteriorates due to



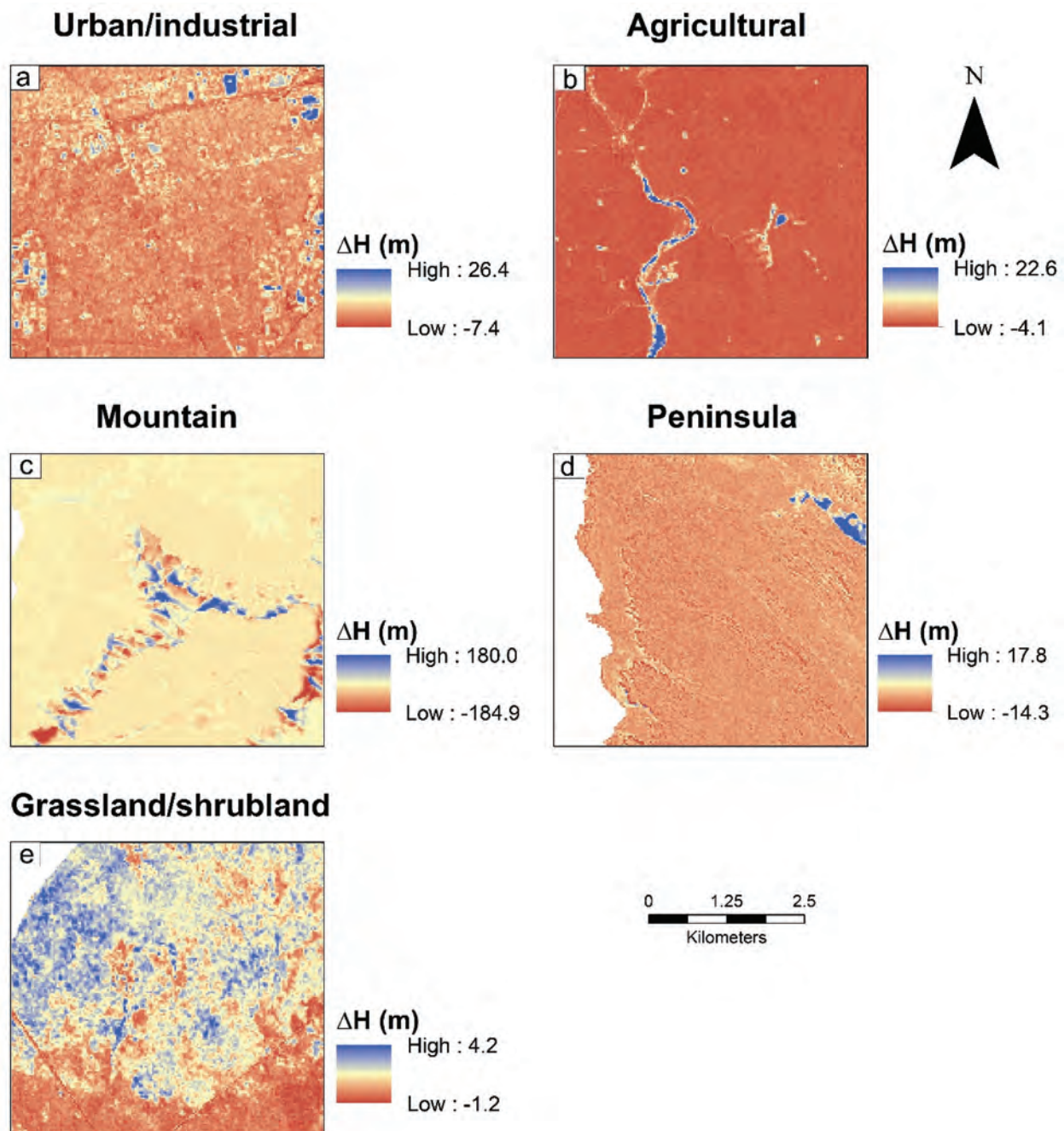


**Figure 15.** Height error maps of the Copernicus DEM at landscapes in Cape Town, (a) urban/industrial (b) agricultural (c) mountain (d) peninsula (e) grassland/shrubland.

the heavy foliage and thick tree canopy cover. The summary of the RMSEs shows that NASADEM had the lowest RMSE (20.28 m), followed by ASTER GDEM (22.08 m), Copernicus (26.13 m) and AW3D (26.65 m). Furthermore, NASADEM was consistent in its performance with the lowest estimated errors in most calculated metrics. ASTER GDEM had the lowest mean error (17.40 m) and the highest NMAD (14.10 m). Based on the ranking results in the forested landscape, NASADEM emerged in first place, followed by ASTER GDEM, Copernicus and AW3D in that order.

The correlations of the elevation errors from the four DEMs are presented in Figure 17. Generally, the elevation

errors from the individual DEMs have a moderate to high positive correlation in the forests (Figures 17(f,g)), and a low to moderate positive correlation in the mountains (Figure 17(c)) and urban areas (Figure 17(a)).

### 3.4. Vertical accuracy by landscape

In the next stage of analysis, we considered the variation in vertical accuracy based on the seven landscapes spread across both locations (Table 6 and Figure 18). Considering the landscapes could reveal the influence of certain terrain peculiarities on the vertical errors. In the urban/industrial, agricultural, mountain and peninsula landscapes, the lowest mean error, SD, RMSE, MAE,

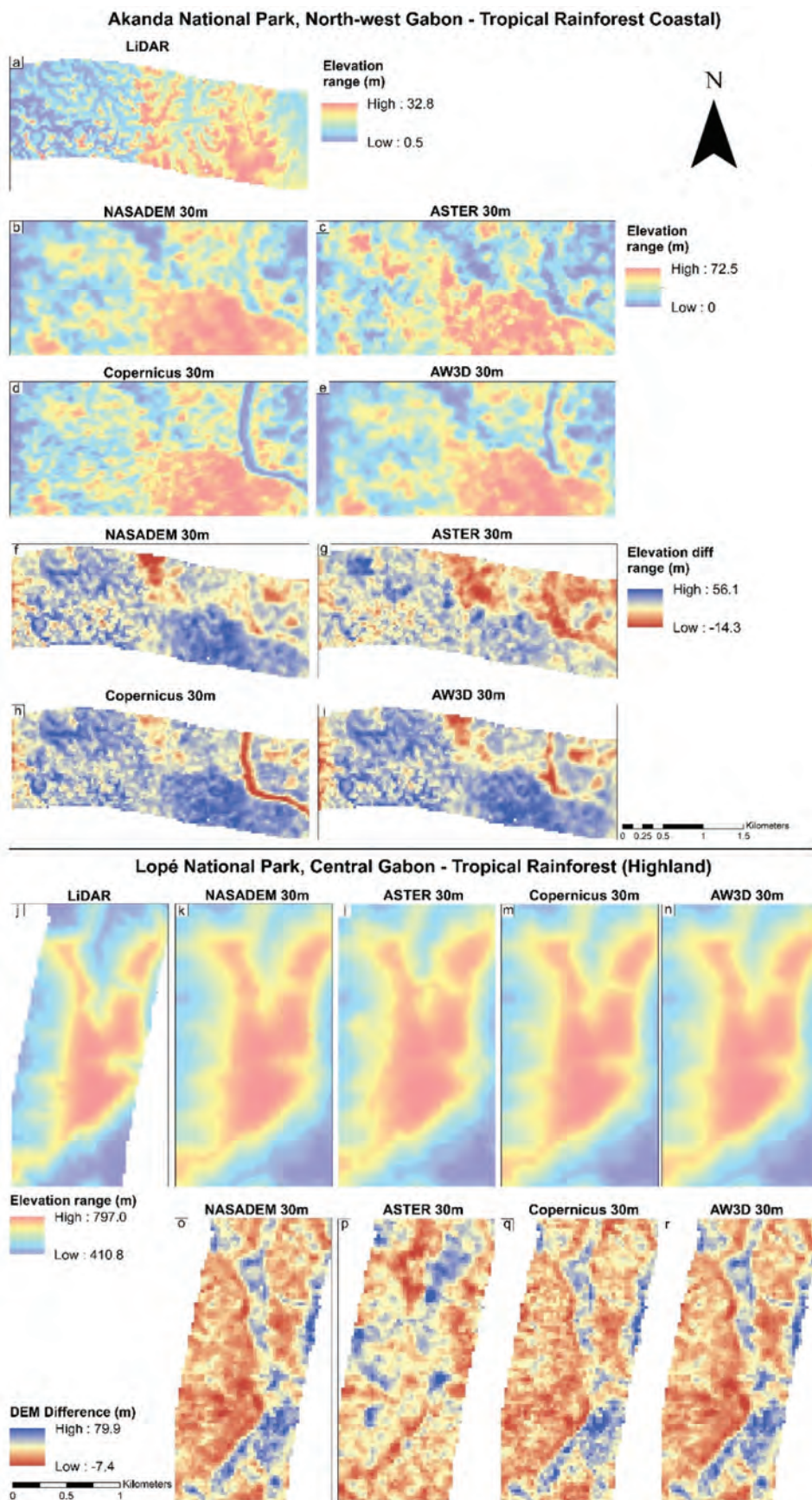
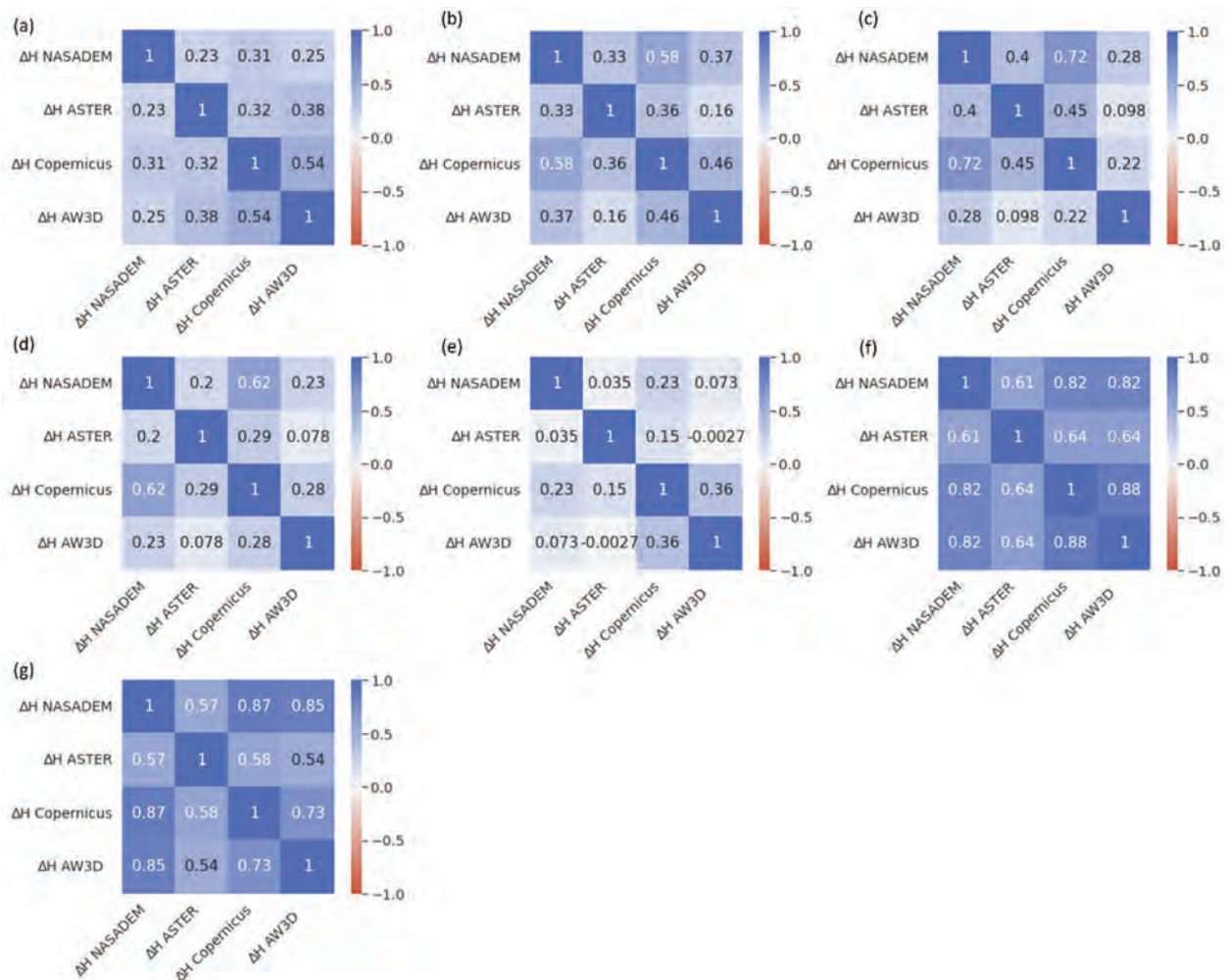


Figure 16. View of the AfriSAR LVIS LiDAR coverage, global DEMs and height error maps at the sites in Gabon.



**Table 5.** Vertical error for all points. The ranks are enclosed in brackets, and the lowest vertical errors are highlighted.

Location	DEM	ME (m)	SD (m)	RMSE (m)	MAE (m)	MAD (m)	NMAD (m)	LE95 (m)	Total Rank	Overall Rank
Cape Town (Whole area)	NASADEM	0.86 (1.03)	3.01 (1.73)	3.13 (1.49)	2.20 (1.49)	1.49 (1.84)	2.21 (1.84)	5.89 (1.73)	11.15	1.59
	ASTER	-4.56 (4.00)	5.55 (4.00)	7.18 (4.00)	5.94 (4.00)	3.32 (4.00)	4.93 (4.00)	10.87 (4.00)	28.00	4.00
	Copernicus	<b>0.82</b> <b>(1.00)</b>	<b>2.19</b> <b>(1.00)</b>	<b>2.34</b> <b>(1.00)</b>	<b>1.47</b> <b>(1.00)</b>	<b>0.78</b> <b>(1.00)</b>	<b>1.16</b> <b>(1.00)</b>	<b>4.29</b> <b>(1.00)</b>	<b>7.00</b>	<b>1.00</b>
	AW3D	2.92 (2.68)	2.31 (1.10)	3.72 (1.86)	3.15 (2.13)	0.99 (1.25)	1.47 (1.25)	4.52 (1.10)	11.38	1.63
Akanda and Lopé National Parks, (Whole area)	NASADEM	18.05 (1.30)	<b>9.25</b> <b>(1.00)</b>	<b>20.28</b> <b>(1.00)</b>	<b>18.13</b> <b>(1.00)</b>	<b>6.19</b> <b>(1.00)</b>	<b>9.18</b> <b>(1.00)</b>	<b>18.13</b> <b>(1.00)</b>	<b>7.30</b>	<b>1.00</b>
	ASTER	<b>17.40</b> <b>(1.00)</b>	13.59 (4.00)	22.08 (1.84)	18.34 (1.11)	9.51 (4.00)	14.10 (4.00)	26.63 (4.00)	19.96	3.63
	Copernicus	23.19 (3.65)	12.06 (2.94)	26.13 (3.76)	23.23 (3.62)	7.67 (2.34)	11.38 (2.34)	23.64 (2.94)	21.59	3.96
	AW3D	23.96 (4.00)	11.68 (2.68)	26.65 (4.00)	23.97 (4.00)	7.52 (2.20)	11.15 (2.20)	22.88 (2.68)	21.76	4.00

**Figure 17.** Correlations between the elevation errors of the four DEMs, after outlier filtering (a) urban/industrial (b) agricultural (c) mountain (d) peninsula (e) grassland/shrubland (f) tropical rainforest – coastal (g) tropical rainforest – highland.

NMAD and linear error were observed in Copernicus DEM. However, in the grassland/shrubland landscape, NASADEM had the lowest ME (-0.36 m), RMSE (1.20 m) and MAE (0.95 m); AW3D had the lowest NMAD of 0.77 m while Copernicus showed the least error dispersion with an SD of 0.81 m. For Copernicus DEM in the Cape Town area, the lowest RMSE of 1.36 m was observed in the Cape Peninsula, while the highest

RMSE of 4.42 m was observed in the mountainous region. ASTER GDEM is ranked as the poorest DEM in Cape Town. This is not surprising as previous accuracy assessment studies have proved the unfavorable performance of ASTER GDEM in several landscapes around the world (e.g. Altunel, Okolie, and Kurtipek 2022; Uemaa et al. 2020). Conversely, some recent studies have asserted the high quality of Copernicus DEM in



**Table 6.** Vertical error based on landscape. The ranks are enclosed in brackets, and the lowest vertical errors are highlighted.

Landscape	DEM	ME (m)	SD (m)	RMSE (m)	MAE (m)	MAD (m)	NMAD (m)	LE95 (m)	Total Rank	Overall Rank
Urban/Industrial	NASADEM	1.35 (1.06)	1.85 (1.49)	2.29 (1.31)	1.85 (1.44)	1.13 (1.81)	1.67 (1.81)	3.63 (1.49)	10.40	1.50
	ASTER	-3.60 (3.23)	3.86 (4.00)	5.28 (4.00)	4.41 (4.00)	2.43 (4.00)	3.60 (4.00)	7.57 (4.00)	27.23	4.00
	Copernicus	<b>1.29</b> <b>(1.00)</b>	<b>1.46</b> <b>(1.00)</b>	<b>1.95</b> <b>(1.00)</b>	<b>1.41</b> <b>(1.00)</b>	<b>0.65</b> <b>(1.00)</b>	<b>0.96</b> <b>(1.00)</b>	<b>2.86</b> <b>(1.00)</b>	<b>7.00</b>	<b>1.00</b>
	AW3D	4.39 (4.00)	1.89 (1.54)	4.78 (3.55)	4.40 (3.99)	0.83 (1.31)	1.23 (1.31)	3.71 (1.54)	17.26	2.52
Agricultural	NASADEM	0.51 (1.14)	2.12 (1.85)	2.18 (1.33)	1.59 (1.37)	1.18 (2.14)	1.76 (2.14)	4.15 (1.85)	11.82	1.69
	ASTER	-7.45 (4.00)	3.92 (4.00)	8.41 (4.00)	7.63 (4.00)	2.43 (4.00)	3.61 (4.00)	7.67 (4.00)	28.00	4.00
	Copernicus	<b>0.17</b> <b>(1.00)</b>	<b>1.41</b> <b>(1.00)</b>	<b>1.42</b> <b>(1.00)</b>	<b>0.74</b> <b>(1.00)</b>	<b>0.42</b> <b>(1.00)</b>	<b>0.62</b> <b>(1.00)</b>	<b>2.76</b> <b>(1.00)</b>	<b>7.00</b>	<b>1.00</b>
	AW3D	2.37 (1.91)	1.53 (1.15)	2.82 (1.60)	2.42 (1.73)	0.78 (1.54)	1.16 (1.54)	3.00 (1.15)	10.62	1.52
Mountain	NASADEM	1.57 (1.46)	5.11 (1.75)	5.35 (1.66)	4.19 (1.72)	3.23 (2.05)	4.78 (2.05)	10.02 (1.75)	12.43	1.78
	ASTER	-4.01 (4.00)	7.65 (4.00)	8.63 (4.00)	6.67 (4.00)	4.47 (4.00)	6.63 (4.00)	14.99 (4.00)	28.00	4.00
	Copernicus	<b>1.13</b> <b>(1.00)</b>	<b>4.27</b> <b>(1.00)</b>	<b>4.42</b> <b>(1.00)</b>	<b>3.40</b> <b>(1.00)</b>	<b>2.56</b> <b>(1.00)</b>	<b>3.79</b> <b>(1.00)</b>	<b>8.37</b> <b>(1.00)</b>	<b>7.00</b>	<b>1.00</b>
	AW3D	3.33 (3.29)	4.33 (1.05)	5.47 (1.74)	4.41 (1.92)	2.59 (1.04)	3.83 (1.04)	8.49 (1.05)	11.15	1.59
Peninsula	NASADEM	0.99 (2.16)	2.03 (1.58)	2.26 (1.67)	1.68 (1.74)	1.07 (1.72)	1.58 (1.72)	3.97 (1.58)	12.17	1.74
	ASTER	-2.29 (4.00)	4.85 (4.00)	5.36 (4.00)	4.40 (4.00)	3.01 (4.00)	4.46 (4.00)	9.51 (4.00)	28.00	4.00
	Copernicus	<b>0.17</b> <b>(1.00)</b>	<b>1.35</b> <b>(1.00)</b>	<b>1.36</b> <b>(1.00)</b>	<b>0.80</b> <b>(1.00)</b>	<b>0.46</b> <b>(1.00)</b>	<b>0.68</b> <b>(1.00)</b>	<b>2.64</b> <b>(1.00)</b>	<b>7.00</b>	<b>1.00</b>
	AW3D	2.14 (3.79)	1.44 (1.08)	2.58 (1.92)	2.24 (2.20)	0.57 (1.14)	0.85 (1.14)	2.83 (1.08)	12.34	1.76
Grassland/Shrubland	NASADEM	<b>-0.36</b> <b>(1.00)</b>	1.15 (1.42)	<b>1.20</b> <b>(1.00)</b>	<b>0.95</b> <b>(1.00)</b>	0.76 (1.48)	1.12 (1.48)	2.25 (1.42)	8.81	1.11
	ASTER	-6.83 (4.00)	3.21 (4.00)	7.55 (4.00)	6.96 (4.00)	1.99 (4.00)	2.94 (4.00)	6.30 (4.00)	28.00	4.00
	Copernicus	1.36 (1.46)	<b>0.81</b> <b>(1.00)</b>	1.58 (1.18)	1.40 (1.22)	0.57 (1.09)	0.84 (1.09)	<b>1.59</b> <b>(1.00)</b>	<b>8.05</b>	<b>1.00</b>
	AW3D	4.09 (2.73)	0.82 (1.02)	4.17 (2.40)	4.09 (2.57)	<b>0.52</b> <b>(1.00)</b>	<b>0.77</b> <b>(1.00)</b>	1.61 (1.02)	11.74	1.55
Tropical Rainforest (Coastal)	NASADEM	18.46 (4.00)	<b>10.10</b> <b>(1.00)</b>	21.05 (4.00)	18.47 (4.00)	7.52 (2.93)	11.15 (2.93)	<b>19.80</b> <b>(1.00)</b>	19.87	3.04
	ASTER	<b>8.96</b> <b>(1.00)</b>	10.37 (1.64)	<b>13.71</b> <b>(1.00)</b>	<b>10.71</b> <b>(1.00)</b>	<b>6.08</b> <b>(1.00)</b>	<b>9.01</b> <b>(1.00)</b>	20.33 (1.64)	<b>8.29</b>	<b>1.00</b>
	Copernicus	13.00 (2.28)	10.83 (2.74)	16.92 (2.31)	13.12 (1.93)	7.95 (3.51)	11.79 (3.51)	21.24 (2.74)	19.03	2.89
	AW3D	15.62 (3.10)	11.36 (4.00)	19.31 (3.29)	15.65 (2.91)	8.31 (4.00)	12.33 (4.00)	22.27 (4.00)	25.30	4.00
Tropical Rainforest (Highland)	NASADEM	<b>17.81</b> <b>(1.00)</b>	8.70 (1.41)	<b>19.82</b> <b>(1.00)</b>	<b>17.93</b> <b>(1.00)</b>	5.33 (1.33)	7.90 (1.33)	17.05 (1.41)	<b>8.47</b>	<b>1.00</b>
	ASTER	22.37 (2.20)	12.78 (4.00)	25.76 (2.71)	22.84 (2.31)	8.28 (4.00)	12.28 (4.00)	25.05 (4.00)	23.22	4.00
	Copernicus	29.19 (4.00)	<b>8.06</b> <b>(1.00)</b>	30.28 (4.00)	29.19 (4.00)	<b>4.97</b> <b>(1.00)</b>	<b>7.37</b> <b>(1.00)</b>	<b>15.79</b> <b>(1.00)</b>	16.00	2.53
	AW3D	28.87 (3.92)	8.68 (1.40)	30.15 (3.96)	28.88 (3.92)	5.31 (1.31)	7.87 (1.31)	17.02 (1.40)	17.21	2.78

terms of vertical accuracy, the accuracy of terrain derivatives, landscape representation, and consistency with its nominal quality specifications (e.g. Li et al. 2022; Purinton and Bookhagen 2021; Valle et al. 2022). In summary, Copernicus DEM emerged with the overall best performance in all five land and terrain conditions within Cape Town.

The trend is different in the densely forested Gabon landscape. Surprisingly, ASTER GDEM performed relatively better than the other DEMs in the coastal forests. The coastal plains are low-lying wetlands and mixed forests straddling the coast. In this landscape, if the RMSE is used as a basis of accuracy, then ASTER

GDEM is the most accurate DEM followed by Copernicus, AW3D and NASADEM in that order. However, in the forested highlands, NASADEM emerged as the most accurate with an RMSE of 19.82 m, followed by ASTER (25.76 m), AW3D (30.15 m) and Copernicus (30.28 m). In the overall ranking for the coastal forests, ASTER GDEM was ranked highest, followed by Copernicus, NASADEM and AW3D in that order. In the forested highlands, NASADEM was ranked highest followed by Copernicus, AW3D and ASTER in that order. Hawker et al. (2022) have shown that in forested areas with canopy cover >50%, the RMSE of Copernicus DEM can exceed 25 m. In another study by Li et al.

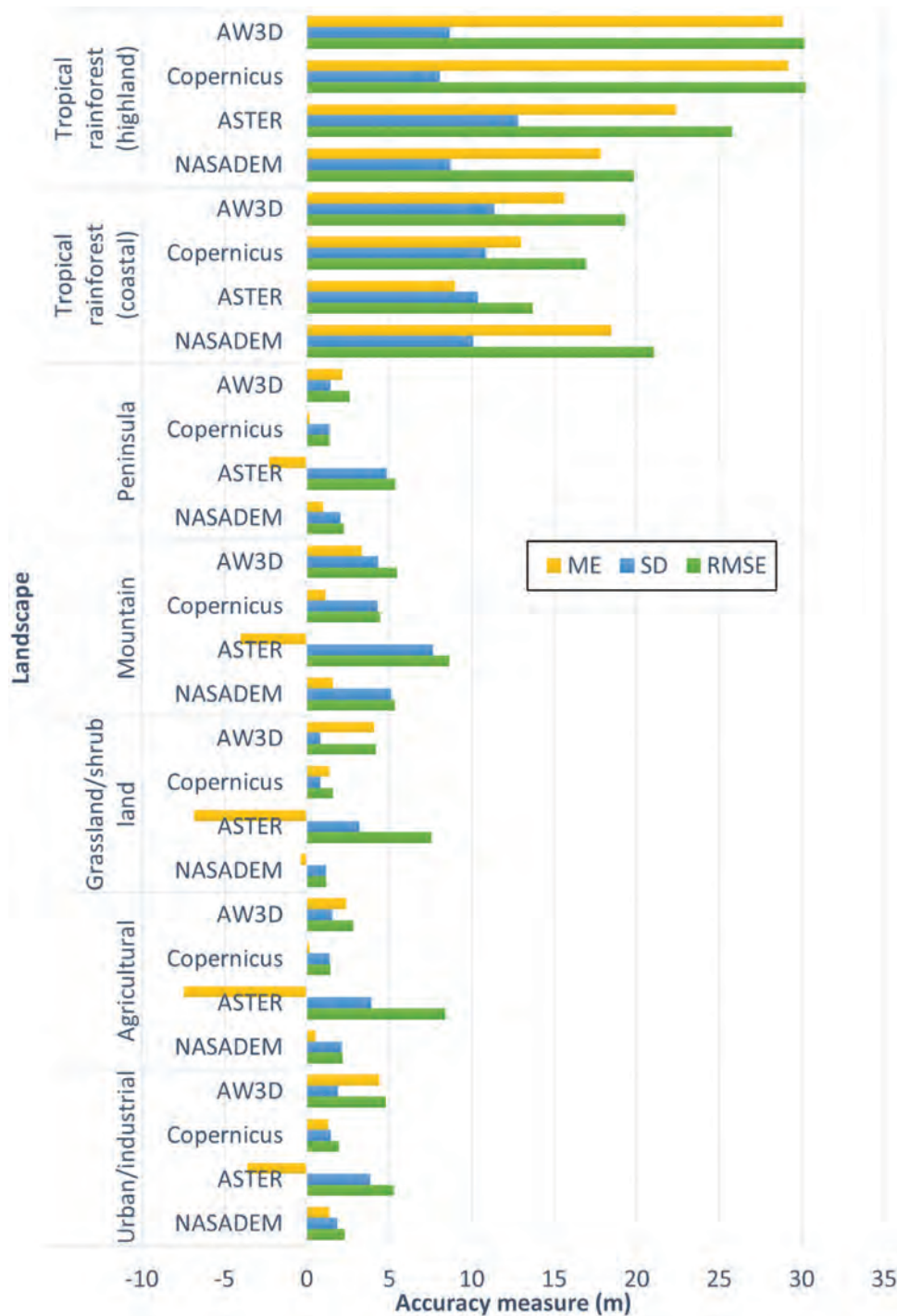


Figure 18. Visualisation of the mean error, SD and RMSE in different landscapes.

(2022), NASADEM had the best accuracy in dense forest, while Copernicus DEM performed the best in bare land and sparse vegetation. Going further, they posited that this may be related to the capability of the C-band SAR of NASADEM for penetrating deeper into vegetation compared to the X-band of Copernicus DEM and the optical band of AW3D30.

### 3.5. Influence of tree cover on vertical accuracy

Figure 19 shows the percentage tree cover maps for Akanda and Lopé in Gabon. Adapting the forest cover

classification of FRIENVIS (2015) and FSI (2021), the percentage tree cover was categorized into the following four classes: very dense (70% and above), dense (40–70%), moderately dense (10–40%), and light (less than 10%). Table 7 shows the calculated accuracy measures based on percentage tree cover.

The DEMs perform best in areas with the least tree cover (<10%, 10–40%), and this is where Copernicus DEM outperforms most DEMs. Using the RMSE as a basis, ASTER showed the highest vertical accuracy in tree cover between 40–70% with the lowest RMSE of 15.10 m. ASTER

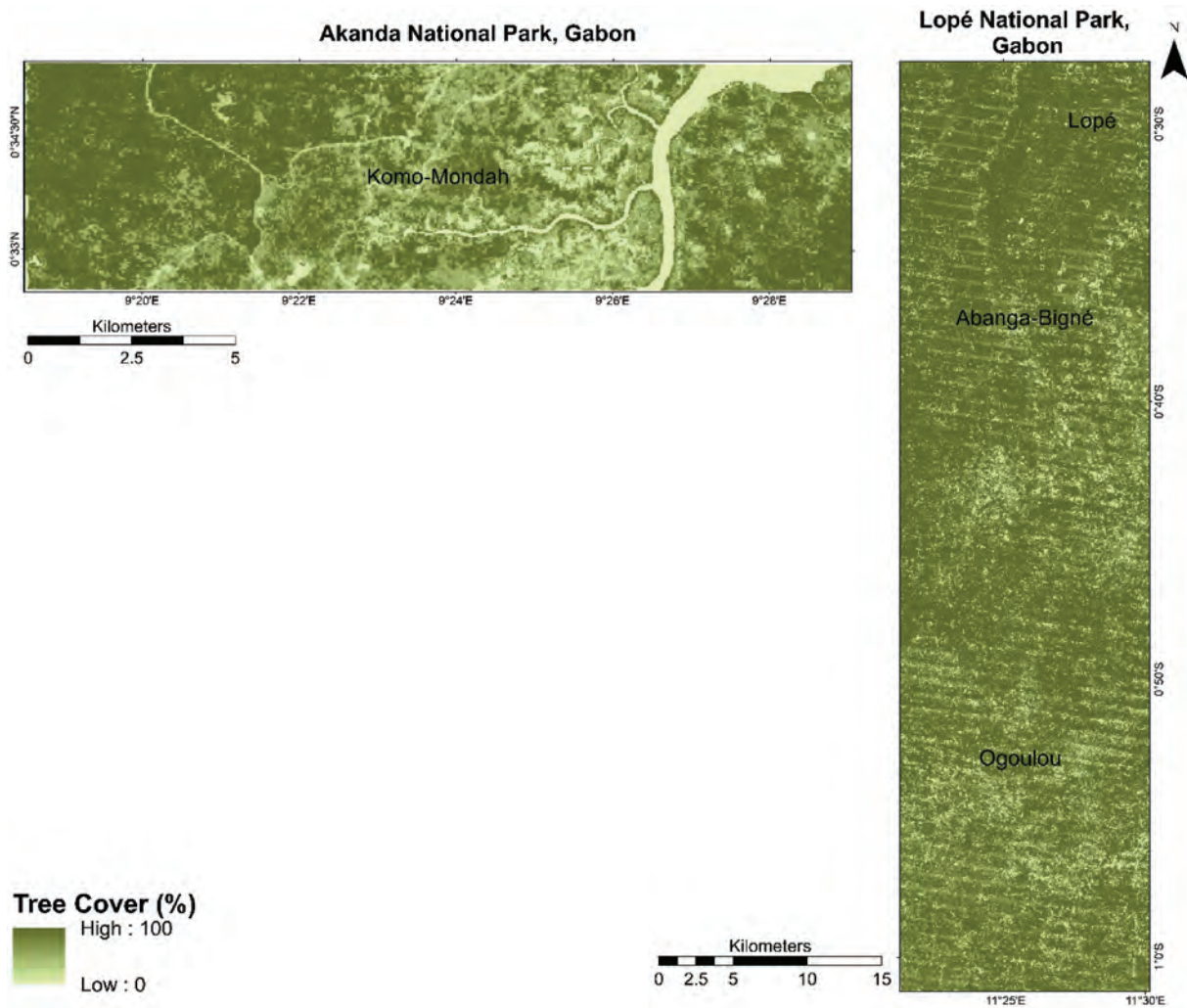


Figure 19. Percentage tree cover maps of the forests at Akanda and Lopé, Gabon.

consistently has a negative bias at most sites (as seen in Table 6), so its “better” performance in dense tree cover is probably due to its overall negative bias. NASADEM provides the best estimates in forests with tree cover >70%, with an RMSE of 20.79 m. However, in all instances where tree cover was greater than 10%, NASADEM

displayed the highest precision and least dispersion (lowest SD) in the elevation errors. Unlike the other DEMs, the raw data for NASADEM was acquired during a relatively narrow temporal period (February 11–22, 2000), and this could have minimized the influence of vegetation seasonal variability on the data accuracy.

Table 7. Vertical error based on percentage tree cover in Akanda and lopé, Gabon. The lowest vertical errors are highlighted.

Tree cover (%)	N	DEM	ME	SD	RMSE	MAE
<10	624	NASADEM	14.13	8.58	16.53	14.13
		ASTER	2.15	8.95	9.20	7.31
		Copernicus	<b>1.70</b>	<b>4.93</b>	<b>5.21</b>	<b>2.70</b>
		AW3D	6.12	8.47	10.44	6.33
10–40	9451	NASADEM	12.05	<b>7.76</b>	14.33	12.08
		ASTER	7.31	11.54	13.66	10.19
		Copernicus	<b>6.32</b>	11.02	<b>12.70</b>	<b>6.69</b>
		AW3D	8.68	10.82	13.87	8.73
40–70	71215	NASADEM	14.50	<b>8.45</b>	16.79	14.53
		ASTER	<b>8.61</b>	12.41	<b>15.10</b>	11.21
		Copernicus	10.78	12.14	16.23	<b>10.99</b>
		AW3D	12.90	11.90	17.54	12.96
>70	544358	NASADEM	<b>18.63</b>	<b>9.23</b>	<b>20.79</b>	<b>18.71</b>
		ASTER	18.74	13.25	22.96	19.43
		Copernicus	25.13	10.79	27.34	25.14
		AW3D	25.69	10.61	27.80	25.70

\*No of points.

### 3.6. Vertical accuracy by slope and aspect

In this section, the relationship of the vertical error with slope and aspect in Cape Town is analyzed. The terrain heterogeneity of Cape Town provides ample opportunity to understand the influence of slope on the vertical accuracy. Guidance on slope classification is available from various sources (e.g. CanSIS 2013; Chesworth et al. 2008). Summarily, we grouped the slope and aspect maps derived from the LiDAR DEM of Cape Town into six slope classes and eight cardinal directions respectively (Supplementary Figure S7). Thereafter, the elevation errors in the four satellite DEMs were

grouped according to these classes. The vertical error based on slope and aspect are shown in Supplementary Tables S2 and S3, and visualized in Figures 20 and 21 respectively. The highest accuracies for all the DEMs occur in flat/gentle areas. As the slope progresses from flat/gentle to moderate; the SD, RMSE, and MAE of Copernicus DEM almost increases by a factor of two. Generally, the DEM accuracies continue to degrade as the steepness increases, and are lowest in excessively steep slopes. The error of Copernicus is the lowest while ASTER is the highest for most slope categories. Even in the steep, very steep, extremely and excessively steep slopes, the RMSE of Copernicus DEM is better

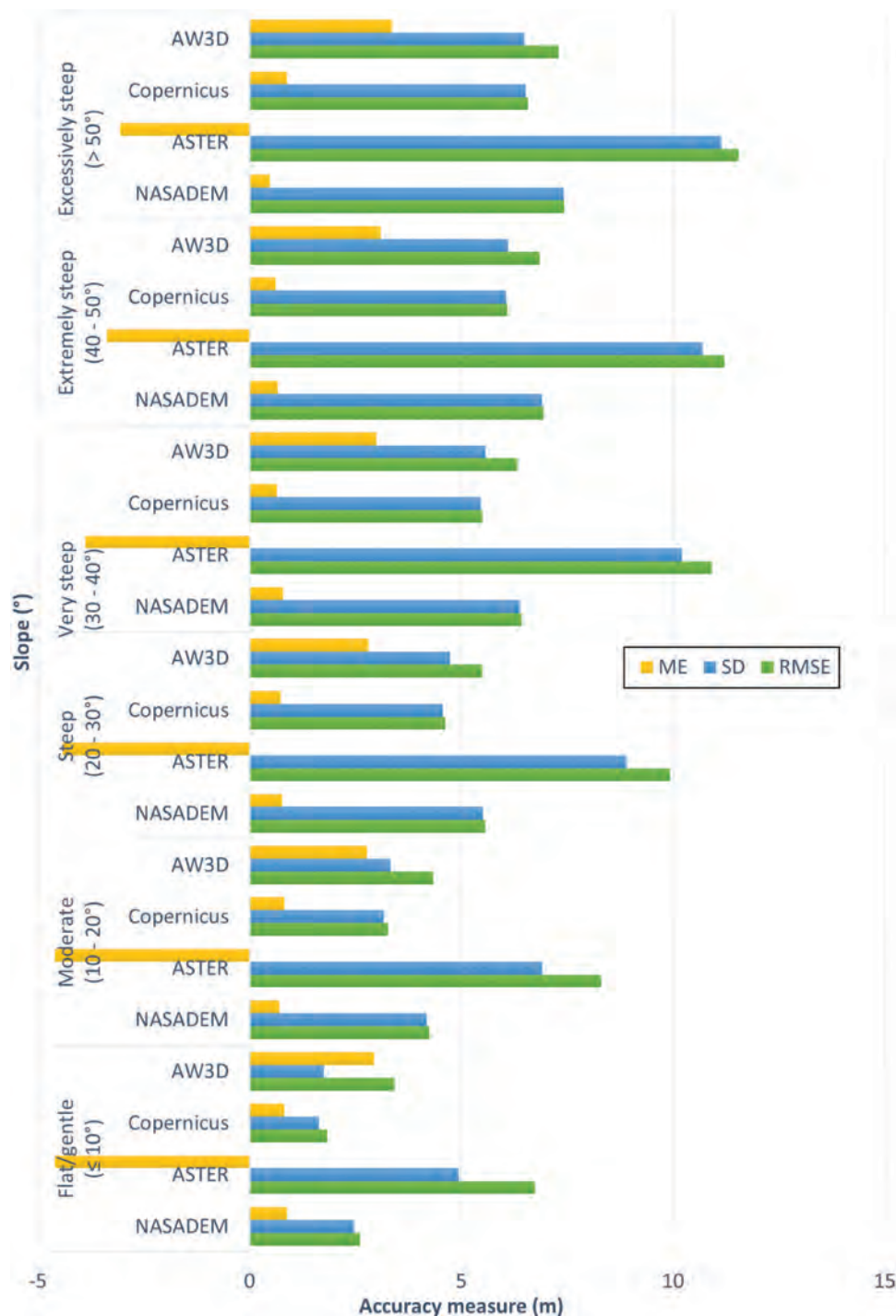
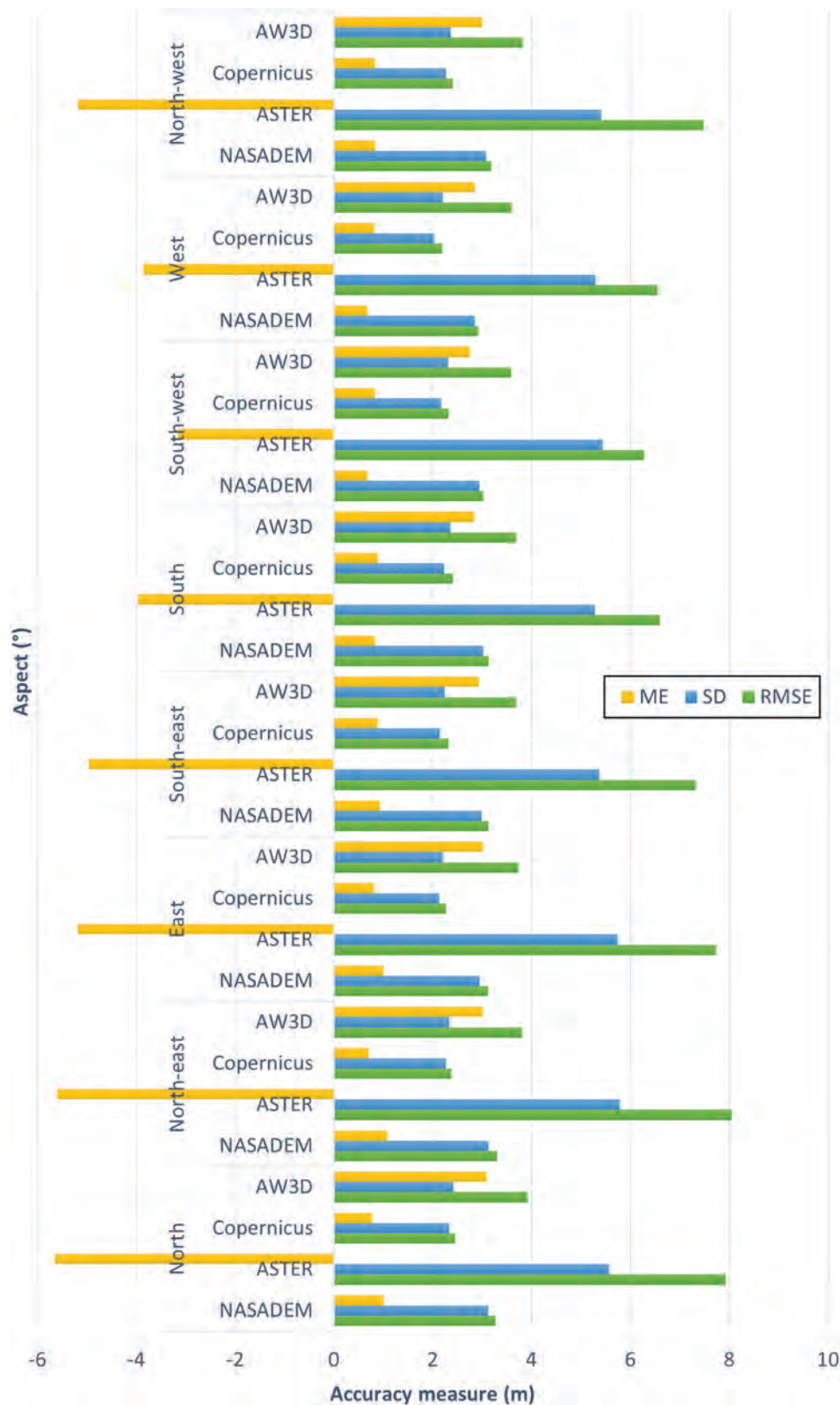


Figure 20. Visualisation of the mean error, SD and RMSE based on slope.





**Figure 21.** Visualisation of the mean error, SD and RMSE based on aspect.

than that of ASTER in the gentle slopes. Similarly, the ME, RMSE and MAE of NASADEM and AW3D in steep and very steep slopes exhibit superior performance to that of ASTER in gentle slopes. Although previous studies have proved the poor reliability of ASTER, these findings highlight that its accuracy is not comparable to counterpart DEMs within the same

slope category. The general trend shows a degradation in DEM accuracy at higher slopes. DEM accuracy is associated with aspect (Nwilo et al. 2022). In the analysis of aspect (Figure 21), the lowest vertical errors across all four DEMs are generally in the west direction, while some particularly higher errors are spotted in the northerly directions (north, northeast, and north-west).

Copernicus emerges as the most accurate with the least SD, RMSE and MAE in most directions, while ASTER GDEM is the least accurate. The largest mean errors are observed in ASTER followed by AW3D.

#### 4. Conclusion and recommendations

The presented study has demonstrated that Copernicus GLO-30 is ranked highest in accuracy in the urban/industrial, agricultural, mountain, peninsula and grasslands/shrubland landscapes. However, ASTER GDEM and NASADEM ranked higher in the low-relief and high-relief tropical forests, respectively. Generally, the height errors from the individual DEMs have a moderate to high positive correlation in forests, and a low to moderate positive correlation in mountains and urban areas. Judging by already established indices for evaluating DEMs, Copernicus DEM clearly outperformed all other DEMs at most sites. NASADEM and AW3D trail behind Copernicus in Cape Town while ASTER GDEM's performance is below expectations, and appears to show considerable negative bias. In the heavily forested Akanda and Lopé National Parks, the performance of the DEMs are quite different. ASTER GDEM's comparable performance with the likes of Copernicus and AW3D in dense tropical forest is possibly an artifact of its overall negative bias. NASADEM which is ranked second in Cape Town, outperformed the other three DEMs in the forested highlands.

This study has provided an extensive validation of these recent versions of NASADEM, ASTER, Copernicus and AW3D DEMs to guide practitioners on their respective limitations for numerous applications. The multi-level analysis goes beyond the reliance on global uncertainty measures by analyzing localized differences through terrain visualization. The study provides a further impetus for national mapping agencies especially in data-sparse regions to implement deliberate measures aimed at exploiting global DEMs for updating topographic maps and databases. Moreover, the assessment methodology is robust and easy-to-follow and can be adapted by other researchers for performing similar studies. Accuracy assessments can be extended to cover other difficult or inaccessible regions such as the Arctic. Future directions of research include comparative hydrological and geo-morphometric analysis of satellite-derived DEMs, and strategies for enhancing or improving DEM accuracies.

#### Acknowledgements

We are grateful to the Chief Directorate: National Geospatial Information (CD: NGI), South Africa for providing us with information on the vertical datum for South Africa. LIDAR data for the City of Cape Town was provided by the Information and Knowledge Management

Department, City of Cape Town. Special thanks to Professor Jennifer Whittal, Dr Isaac Apeh and Dr Siphwe Mphuthi for their valuable comments. Lastly, we thank the journal Editors and reviewers for their feedback which improved the quality of the article.

#### Disclosure statement

No potential conflict of interest was reported by the author(s).

#### Funding

This work is supported by the (i) Commonwealth Scholarship Commission and the Foreign, Commonwealth and Development Office in the UK [Grant number NGCN-2021-239] (ii) University of Cape Town Postgraduate Funding Office. We are grateful for their support. All views expressed here are those of the author(s) not the funding bodies.

#### Notes on contributors

*Chukwuma Okolie* is a PhD candidate at the Geomatics Division, University of Cape Town South Africa. His research interests are geospatial data science and artificial intelligence, data fusion, GIScience, remote sensing and environmental modelling.

*Jon Mills* is a Professor of Geomatic Engineering at Newcastle University, UK. His research interests are photogrammetric computer vision and laser scanning.

*Adedayo Adeleke* is a Lecturer at the University of Pretoria South Africa. His research interests are data fusion, deep learning raster analysis, and site suitability analysis.

*Julian Smit* is a Director at AfriMap Geo-Information Services, South Africa. His research interests are remote sensing, photogrammetry, environmental systems monitoring and modelling, and spatial data science.

*Maria Peppia* is a Lecturer in Geospatial Engineering, Newcastle University UK. Her research interest are UAV photogrammetry and earth observations.

*Arif Altunel* is an Associate Professor in the Faculty of Forestry, Kastamonu University, Türkiye. His research interests are topography, land cover, terrain modelling and forestry.

*Ikenna Arungwa* is a Lecturer at the Federal University of Technology, Owerri, Nigeria. His research interests are geodesy and geomatics.

#### ORCID

Chukwuma J. Okolie  <http://orcid.org/0000-0003-4542-7051>

Jon P. Mills  <http://orcid.org/0000-0001-5304-7935>

Adedayo K. Adeleke  <http://orcid.org/0000-0002-4783-0576>

Julian L. Smit  <http://orcid.org/0000-0001-8664-8059>

Maria V. Peppia  <http://orcid.org/0000-0001-9683-0217>

Arif O. Altunel  <http://orcid.org/0000-0003-2597-5587>

Ikenna D. Arungwa  <http://orcid.org/0000-0002-3946-2953>

## Author contributions

Chukwuma Okolie: conceptualization, manuscript writing – original draft, review and editing, methodology, data curation, investigation, visualization, formal analysis.

Jon Mills: conceptualization, manuscript review and editing, resources, validation, supervision.

Adedayo Adeleke: conceptualization, manuscript review and editing, validation, supervision.

Julian Smit: conceptualization, manuscript review and editing, resources, validation, supervision.

Maria Peppia: manuscript review and editing, resources, validation.

Arif Altunel: manuscript review and editing, formal analysis.

Ikenna Arungwa: manuscript review and editing, formal analysis.

## Data availability statement

The data that support the findings of this study are available from the corresponding author upon reasonable request.

## References

- Abrams, M., R. Crippen, and H. Fujisada. 2020. “ASTER Global Digital Elevation Model (GDEM) and ASTER Global Water Body Dataset (ASTWBD).” *Remote Sensing* 12 (7): 1156. <https://doi.org/10.3390/RS12071156>.
- Airbus. 2020a. “Copernicus DEM Copernicus Digital Elevation Model Product Handbook.”
- Airbus. 2020b. “Copernicus DEM Copernicus Digital Elevation Model Validation Report.”
- Altunel, A. O. 2021. “Questioning the Effects of Raster-Resampling and Slope on the Precision of TanDEM-X 90 M Digital Elevation Model.” *Geocarto international* 36 (20): 2366–2382.
- Altunel, A. O., C. J. Okolie, and A. Kurtipek. 2022. “Capturing the Level of Progress in Vertical Accuracy Achieved by ASTER GDEM Since the Beginning: Turkish and Nigerian Examples.” *Geocarto International* 37 (26): 12073–12095. <https://doi.org/10.1080/10106049.2022.2063409>.
- Banerjee, K., M. B. Santhosh Kumar, and L. N. Tilak. 2022. “Effectiveness of Digital Elevation Models in Morphometric Analysis Using Remote Sensing and GIS Approach for Smart Society.” *Decision Analytics for Sustainable Development in Smart Society* 5:153–172. [https://doi.org/10.1007/978-981-19-1689-2\\_10](https://doi.org/10.1007/978-981-19-1689-2_10).
- Barrand, N. E., T. Murray, T. D. James, S. L. Barr, and J. P. Mills. 2009. “Optimizing Photogrammetric DEMs for Glacier Volume Change Assessment Using Laser-Scanning Derived Ground-Control Points.” *Journal of Glaciology* 55 (189): 106–116. <https://doi.org/10.3189/002214309788609001>.
- Benahmed Daho, S. A. 2009. “Evaluation of the Earth Gravity Model EGM2008 in Algeria.”
- Blair, J. B., and M. Hofton. 2018. “AfriSar LVIS L2 Geolocated Surface Elevation Product, Version 1.” NASA National Snow and Ice Data Center Distributed Active Archive Center. <https://doi.org/10.5067/A0PMUXXVUYNH>.
- Blair, J. B., D. L. Rabine, and M. A. Hofton. 1999. “The Laser Vegetation Imaging Sensor: A Medium-Altitude, Digitisation-Only, Airborne Laser Altimeter for Mapping Vegetation and Topography.” *ISPRS Journal of Photogrammetry and Remote Sensing* 54 (2–3): 115–122. [https://doi.org/10.1016/S0924-2716\(99\)00002-7](https://doi.org/10.1016/S0924-2716(99)00002-7).
- Bove, G., A. Becker, B. Sweeney, M. Vousdoukas, and S. Kulp. 2020. “A Method for Regional Estimation of Climate Change Exposure of Coastal Infrastructure: Case of USVI and the Influence of Digital Elevation Models on Assessments.” *Science of the Total Environment* 710:136162. <https://doi.org/10.1016/J.SCITOTENV.2019.136162>.
- Buckley, S. M., P. S. Agram, J. E. Belz, R. E. Crippen, E. M. Gurrola, S. Hensley, M. Kobrick, et al. 2020. “NASADEM: User Guide.” [https://lpdaac.usgs.gov/documents/592/NASADEM\\_User\\_Guide\\_V1.pdf](https://lpdaac.usgs.gov/documents/592/NASADEM_User_Guide_V1.pdf).
- CanSIS (Canadian Soil Information Service). 2013. “Slope Gradient.” <https://sis.agr.gc.ca/cansis/nsdb/slc/v3.2/cmp/slope.html>.
- Carrera-Hernández, J. J. 2021. “Not All DEMs are Equal: An Evaluation of Six Globally Available 30 M Resolution DEMs with Geodetic Benchmarks and LiDar in Mexico.” *Remote Sensing of Environment* 261:112474. <https://doi.org/10.1016/J.RSE.2021.112474>.
- CCT (City of Cape Town). 2023. “Information and Knowledge Management Department.” <https://www.cape-town.gov.za/Departments/InformationandKnowledgeManagementDepartment>.
- Cenci, L., M. Galli, G. Palumbo, L. Sapia, C. Santella, and C. Albinet. 2021. “Describing the Quality Assessment Workflow Designed for Dem Products Distributed Via the Copernicus Programme. Case Study: The Absolute Vertical Accuracy of the Copernicus Dem Dataset in Spain.” Paper presented at International Geoscience and Remote Sensing Symposium (IGARSS), Brussels, July 11–16.
- Chandler, G., and C. L. Merry. 2010. “The South African Geoid 2010: SAGEOID10.” [https://www.isgeoid.polimi.it/Geoid/Africa/SouthAfrica/sudAfrica\\_g.html](https://www.isgeoid.polimi.it/Geoid/Africa/SouthAfrica/sudAfrica_g.html).
- Chen, L., Y. Che, Y. Cao, S. Wang, and X. Ma. 2022. “Glacier Mass Balance Based on Two Digital Elevation Models and Ground Observation Records for the Baishui River Glacier No. 1 in Yulong Snow Mountain, Southeastern Qinghai–Tibet Plateau.” *Frontiers in Earth Science* 10:696. <https://doi.org/10.3389/feart.2022.883673>.
- Chesworth, W., M. C. Arbestain, F. Macías, O. Spaargaren, Y. Muallem, H. J. Morel-Seytoux, W. R. Horwath, G. Almendros, W. Chesworth, P. R. Gross, D. L. Sparks, et al. 2008. “Classification of Soils: FAO.” In *Encyclopedia of Soil Science*, 111–113. [https://link.springer.com/reference/workentry/10.1007/978-1-4020-3995-9\\_102](https://link.springer.com/reference/workentry/10.1007/978-1-4020-3995-9_102).
- Ebinne, E. S., O. I. Apeh, E. C. Moka, and E. J. Abah. 2022. “Comparative Analysis of Freely Available Digital Elevation Models for Applications in Multi-Criteria Environmental Modeling Over Data Limited Regions.” *Remote Sensing Applications: Society & Environment* 27:100795. <https://doi.org/10.1016/J.RSASE.2022.100795>.
- Emery, W., and A. Camps. 2017. “Orbital Mechanics, Image Navigation, and Cartographic Projections.” *Introduction to Satellite Remote Sensing*, edited by E. William and C. Adriano, 565–596. Elsevier. <https://doi.org/10.1016/B978-0-12-809254-5.00007-5>.
- Epuh, E. E., A. I. Moshood, C. J. Okolie, O. E. Daramola, S. A. Akinnusi, I. D. Arungwa, M. J. Orji, H. O. Olanrewaju, and A. A. Fatoyinbo. 2022. “Integration of Satellite Gravimetry, Multispectral Imagery and Digital Elevation Model for Investigating



- Crustal Deformation in the Niger Delta Basin.” *Geosystems and Geoenvironment* 1 (3): 100067. <https://doi.org/10.1016/J.GEOGEO.2022.100067>.
- Ettritch, G., A. Hardy, L. Bojang, D. Cross, P. Bunting, and P. Brewer. 2018. “Enhancing Digital Elevation Models for Hydraulic Modelling Using Flood Frequency Detection.” *Remote Sensing of Environment* 217:506–522. <https://doi.org/10.1016/J.RSE.2018.08.029>.
- Fatoyinbo, T., J. Armston, M. Simard, S. Saatchi, M. Denbina, M. Lavalley, M. Hofton, et al. 2021. “The NASA AfriSar Campaign: Airborne SAR and Lidar Measurements of Tropical Forest Structure and Biomass in Support of Current and Future Space Missions.” *Remote Sensing of Environment* 264:112533. <https://doi.org/10.1016/J.RSE.2021.112533>.
- Fatoyinbo, L., N. Pinto, M. Hofton, M. Simard, B. Blair, S. Saatchi, Y. Lou, et al. 2017. “The 2016 NASA AfriSar Campaign: Airborne SAR and Lidar Measurements of Tropical Forest Structure and Biomass in Support of Future Satellite Missions.” Paper presented at the International Geoscience and Remote Sensing Symposium (IGARSS), Fort Worth, July 23–28.
- Florinsky, I. V. 2008. “Global Lineaments: Application of Digital Terrain Modelling.” *Advances in Digital Terrain Analysis*, edited by Q. Zhou, B. Lees, and G. Tang, 365–382. Heidelberg: Springer.
- Friedt, J. M., F. Tolle, É. Bernard, M. Griselin, D. Laffly, and C. Marlin. 2012. “Assessing the Relevance of Digital Elevation Models to Evaluate Glacier Mass Balance: Application to Austre Lovénbreen (Spitsbergen, 79°N).” *Polar Record* 48 (1): 2–10. <https://doi.org/10.1017/S0032247411000465>.
- FRIENVIS. 2015. “Forest Cover Classification.” [https://frienvis.nic.in/Database/ForestCoverClassification\\_2241.aspx?format=Print](https://frienvis.nic.in/Database/ForestCoverClassification_2241.aspx?format=Print).
- FSI. 2021. “Forest Cover Mapping.” <https://fsi.nic.in/scheme-of-classification#:~:text=Theforestcoverisbroadly,forest%2Copenforestandmangrove.>
- Gdulová, K., J. Marešová, and V. Moudrý. 2020. “Accuracy Assessment of the Global TanDEM-X Digital Elevation Model in a Mountain Environment.” *Remote Sensing of Environment* 241:111724. <https://doi.org/10.1016/j.rse.2020.111724>.
- Gesch, D. B. 2018. “Best Practices for Elevation-Based Assessments of Sea-Level Rise and Coastal Flooding Exposure.” *Frontiers in Earth Science* 6:230. <https://doi.org/10.3389/feart.2018.00230>.
- Gesch, D. B., M. J. Oimoen, and G. A. Evans. 2014. “Accuracy Assessment of the U.S. Geological Survey National Elevation Dataset, and Comparison with Other Large-Area Elevation Datasets: SRTM and ASTER.” <https://doi.org/10.3133/OFR20141008>.
- GLAD. 2023. “Global 2010 Tree Cover (30 M) | GLAD.” <https://glad.umd.edu/dataset/global-2010-tree-cover-30-m>.
- Goldstein, J. H., H. Tallis, A. Cole, S. Schill, E. Martin, M. Heiner, M. Paiz, A. Aldous, C. Apse, and B. Nickel. 2017. “Spatial Planning for a Green Economy: National-Level Hydrologic Ecosystem Services Priority Areas for Gabon.” *PLoS One* 12 (6): 1–21. <https://doi.org/10.1371/journal.pone.0179008>.
- Goodness, J., and P. M. L. Anderson. 2013. “Local Assessment of Cape Town: Navigating the Management Complexities of Urbanization, Biodiversity, and Ecosystem Services in the Cape Floristic Region.” *Urbanization, Biodiversity and Ecosystem Services: Challenges and Opportunities: A Global Assessment* 461–484. [https://doi.org/10.1007/978-94-007-7088-1\\_24/FIGURES/5](https://doi.org/10.1007/978-94-007-7088-1_24/FIGURES/5).
- Grohmann, C. 2018. “Evaluation of TanDEM-X DEMs on Selected Brazilian Sites: Comparison with SRTM, ASTER GDEM and ALOS AW3D30.” *Remote Sensing of Environment* 212:121–133. <https://doi.org/10.1016/j.rse.2018.04.043>.
- Guth, P. L., and T. M. Geoffroy. 2021. “LiDAR Point Cloud and ICESat-2 Evaluation of 1 Second Global Digital Elevation Models: Copernicus Wins.” *Transactions in GIS* 25 (5): 2245–2261. <https://doi.org/10.1111/TGIS.12825>.
- Hansen, M. C., P. V. Potapov, R. Moore, M. Hancher, S. A. Turubanova, A. Tyukavina, D. Thau, et al. 2013. “High-Resolution Global Maps of 21st-Century Forest Cover Change.” *Science* 342 (6160): 850–853. <https://doi.org/10.1126/science.1244693>.
- Hawker, L., J. Neal, and P. Bates. 2019. “Accuracy Assessment of the TanDEM-X 90 Digital Elevation Model for Selected Floodplain Sites.” *Remote Sensing of Environment* 232:111319. <https://doi.org/10.1016/J.RSE.2019.111319>.
- Hawker, L., P. Uhe, L. Paulo, J. Sosa, J. Savage, C. Sampson, and J. Neal. 2022. “A 30 M Global Map of Elevation with Forests and Buildings Removed.” *Environmental Research Letters* 17 (2): 24016. <https://doi.org/10.1088/1748-9326/AC4D4F>.
- Hille, K. B. 2016. “NASA, Partner Space Agencies Measure Forests in Gabon.” *NASA Website*. <https://www.nasa.gov/technology/nasa-partner-space-agencies-measure-for-ests-in-gabon/>.
- Hofton, M., R. Dubayah, J. B. Blair, and D. Rabine. 2006. “Validation of SRTM Elevations Over Vegetated and Non-Vegetated Terrain Using Medium Footprint Lidar.” *Photogrammetric Engineering and Remote Sensing* 72 (3): 279–285. <https://doi.org/10.14358/PERS.72.3.279>.
- Hofton, M. A., L. E. Rocchio, J. B. Blair, and R. Dubayah. 2002. “Validation of Vegetation Canopy Lidar Sub-Canopy Topography Measurements for a Dense Tropical Forest.” *Journal of Geodynamics* 34 (3–4): 491–502. [https://doi.org/10.1016/S0264-3707\(02\)00046-7](https://doi.org/10.1016/S0264-3707(02)00046-7).
- Höhle, J., and M. Höhle. 2009. “Accuracy Assessment of Digital Elevation Models by Means of Robust Statistical Methods.” *ISPRS Journal of Photogrammetry and Remote Sensing* 64 (4): 398–406. <https://doi.org/10.1016/J.ISPRSJPRS.2009.02.003>.
- Hoja, D., P. Reinartz, and M. Schroeder. 2006. “Comparison of DEM Generation and Combination Methods Using High Resolution Optical Stereo Imagery and Interferometric SAR Data.” *Revue Francaise de Photogrammetrie et de Teledetection* 184:89–94. <https://www.semanticscholar.org/paper/8296f905520fab744b4aa24f41054065471a9569>.
- Hooijer, A., and R. Vernimmen. 2021. “Global LiDAR Land Elevation Data Reveal Greatest Sea-Level Rise Vulnerability in the Tropics.” *Nature Communications* 12 (1): 1–7. <https://doi.org/10.1038/s41467-021-23810-9>.
- Huber, M., N. Osterkamp, U. Marschalk, R. Tubbesing, A. Wendleder, B. Wessel, and A. Roth. 2021. “Shaping the Global High-Resolution TanDEM-X Digital Elevation Model.” *IEEE Journal of Selected Topics in Applied Earth Observations and Remote Sensing* 14:7198–7212. <https://doi.org/10.1109/JSTARS.2021.3095178>.
- IBM. 2023. “IBM SPSS Software.” <https://www.ibm.com/uk-en/spss>.

- Ishola, K. S., A. A. Fatoyinbo, A. I. Hamid-Mosaku, C. J. Okolie, O. E. Daramola, and T. O. Lawal. 2023. "Groundwater Potential Mapping in Hard Rock Terrain Using Remote Sensing, Geospatial and Aeromagnetic Data." *Geosystems and Geoenvironment* 2 (1): 100107. <https://doi.org/10.1016/J.GEOGEO.2022.100107>.
- Jain, S. K., and V. P. Singh. 2003. "Emerging Techniques for Data Acquisition and Systems Modeling." *Developments in Water Science* 51 (C): 123–205. [https://doi.org/10.1016/S0167-5648\(03\)80057-6](https://doi.org/10.1016/S0167-5648(03)80057-6).
- JAXA. 2019. "ALOS Global Digital Surface Model (DSM) ALOS World 3D-30m (AW3D30) Version 2.2 Product Description." [https://www.eorc.jaxa.jp/ALOS/en/aw3d30/aw3d30v22\\_product\\_e.pdf](https://www.eorc.jaxa.jp/ALOS/en/aw3d30/aw3d30v22_product_e.pdf).
- JAXA. n.d. "ALOS Global Digital Surface Model 'ALOS World 3D - 30m' (AW3D30)." Accessed August 5, 2023. <https://www.eorc.jaxa.jp/ALOS/en/dataset/aw3d30/>.
- Kakavas, M. P., and K. G. Nikolakopoulos. 2021. "Digital Elevation Models of Rockfalls and Landslides: A Review and Meta-Analysis." *Geosciences* 11 (6): 256. <https://doi.org/10.3390/GEOSCIENCES11060256>.
- Kasi, V., R. Pinninti, S. R. Landa, M. Rathinasamy, C. Sangamreddi, R. R. Kuppli, and P. R. D. Radha. 2020. "Comparison of Different Digital Elevation Models for Drainage Morphometric Parameters: A Case Study from South India." *Arabian Journal of Geosciences* 13 (19): 1–17. <https://doi.org/10.1007/s12517-020-06049-4>.
- Laurini, R., and D. Thompson. 1992. "Geometries: Position, Representation, Dimensions." *Fundamentals of Spatial Information Systems* 113–174. <https://doi.org/10.1016/B978-0-08-092420-5.50009-8>.
- Lehner, B., K. Verdin, and A. Jarvis. 2008. "New Global Hydrography Derived from Spaceborne Elevation Data." *Eos Transactions American Geophysical Union* 89 (10): 93–94. <https://doi.org/10.1029/2008EO100001>.
- Li, H., J. Zhao, B. Yan, L. Yue, and L. Wang. 2022. "Global DEMs Vary from One to Another: An Evaluation of Newly Released Copernicus, NASA and AW3D30 DEM on Selected Terrains of China Using ICESat-2 Altimetry Data." *International Journal of Digital Earth* 15 (1): 1149–1168. <https://doi.org/10.1080/17538947.2022.2094002>.
- "LP360: LiDAR & Photogrammetry 3D Point Cloud Software". LP360. <https://www.lp360.com/>.
- Mahesh, R., K. J. Sarunjith, S. Rajakumari, R. Muruganandam, and R. Ramesh. 2021. "Quality Assessment of Open Sourced Digital Elevation Models in Southeast Coast of India." *The Egyptian Journal of Remote Sensing & Space Science* 24 (3): 745–754. <https://doi.org/10.1016/J.EJRS.2021.03.006>.
- McClellan, F., R. Dawson, and C. Kilsby. 2020. "Implications of Using Global Digital Elevation Models for Flood Risk Analysis in Cities." *Water Resources Research* 56 (10): 10. <https://doi.org/10.1029/2020WR028241>.
- McNabb, R., C. Nuth, A. Käb, and L. Girod. 2019. "Sensitivity of Glacier Volume Change Estimation to DEM Void Interpolation." *The Cryosphere* 13 (3): 895–910. <https://doi.org/10.5194/TC-13-895-2019>.
- Merry, C. L. 2009. "EGM2008 Evaluation for Africa." *Newton's Bulletin* 200–206. [https://www.isgeoid.polimi.it/Newton/Newton\\_4/Report\\_EA10\\_Africa.pdf](https://www.isgeoid.polimi.it/Newton/Newton_4/Report_EA10_Africa.pdf).
- Mesa-Mingorance, J. L., and F. J. Ariza-López. 2020. "Accuracy Assessment of Digital Elevation Models (DEMs): A Critical Review of Practices of the Past Three Decades." *Remote Sensing* 12 (16): 2630. <https://doi.org/10.3390/RS12162630>.
- Microsoft. 2023. "Microsoft Excel." <https://www.microsoft.com/en-us/microsoft-365/excel>.
- Muthusamy, M., M. R. Casado, D. Butler, and P. Leinster. 2021. "Understanding the Effects of Digital Elevation Model Resolution in Urban Fluvial Flood Modelling." *Canadian Journal of Fisheries and Aquatic Sciences* 596:126088. <https://doi.org/10.1016/J.JHYDROL.2021.126088>.
- NASA. 2020. "Land Vegetation and Ice Sensor." <https://lvis.gsfc.nasa.gov/Data/Maps/Gabon2016Map.html>.
- Ngangorica. 2014. "Elephants in Lopé National Park." <https://commons.wikimedia.org/w/index.php?curid=37721980>.
- Ni, W., K. J. Ranson, Z. Zhang, and G. Sun. 2014. "Features of Point Clouds Synthesized from Multi-View ALOS/PRISM Data and Comparisons with LiDAR Data in Forested Areas." *Remote Sensing of Environment* 149:47–57. <https://doi.org/10.1016/J.RSE.2014.04.001>.
- Ni, W., G. Sun, and K. J. Ranson. 2013. "Characterization of ASTER GDEM Elevation Data Over Vegetated Area Compared with Lidar Data." *International Journal of Digital Earth* 8 (3): 198–211. <https://doi.org/10.1080/17538947.2013.861025>.
- Ni, W., G. Sun, Z. Zhang, Z. Guo, and Y. He. 2014. "Co-Registration of Two DEMs: Impacts on Forest Height Estimation from SRTM and NED at Mountainous Areas." *IEEE Geoscience & Remote Sensing Letters* 11 (1): 273–277. <https://doi.org/10.1109/LGRS.2013.2255580>.
- Nwilo, P. C., C. O. Ogbeta, O. E. Daramola, C. J. Okolie, and M. J. Orji. 2021. "Soil Erosion Susceptibility Mapping of Imo River Basin Using Modified Geomorphometric Prioritisation Method." *Quaestiones Geographicae* 40 (3): 143–162. <https://doi.org/10.2478/QUAGEO-2021-0029>.
- Nwilo, P. C., J. C. Onyegbula, C. J. Okolie, O. E. Daramola, O. E. Abolaji, and I. D. Arungwa. 2022. "Influence of Land Cover, Slope, and Aspect on the Vertical Accuracy of SPOT DEM at Selected Sites in Nigeria." *Applied Geomatics* 14 (1): 17–31. <https://doi.org/10.1007/s12518-021-00404-0>.
- Okolie, C. J., and I. D. Arungwa. 2022. "Accuracy Assessment of ALOS World 3D-30m DEMs Using Field Data from Lagos and Federal Capital Territory, Nigeria." *Geocarto International* 37 (26): 11686–11705. <https://doi.org/10.1080/10106049.2022.2060320>.
- Olajubu, V., M. A. Trigg, C. Berretta, A. Sleigh, M. Chini, P. Matgen, S. Mojere, and J. Mulligan. 2021. "Urban Correction of Global DEMs Using Building Density for Nairobi, Kenya." *Earth Science Informatics* 14 (3): 1383–1398. <https://doi.org/10.1007/s12145-021-00647-w>.
- Oliveira, C. G. D., W. R. Paradella, and A. D. Q. D. Silva. 2011. "Assessment of Radargrammetric DSMs from TerraSAR-X Stripmap Images in a Mountainous Relief Area of the Amazon Region." *ISPRS Journal of Photogrammetry & Remote Sensing* 66 (1): 67–72. <https://doi.org/10.1016/J.ISPRSJPRS.2010.08.008>.
- Orimoloye, I. R., O. O. Ololade, S. P. Mazinyo, A. M. Kalumba, O. Y. Ekundayo, E. T. Busayo, A. A. Akinsanola, and W. Nel. 2019. "Spatial Assessment of Drought Severity in Cape Town Area, South Africa." *Heliyon* 5 (7): e02148. <https://doi.org/10.1016/J.HELIYON.2019.E02148>.
- Pavlis, N. K., S. A. Holmes, S. C. Kenyon, and J. K. Factor. 2012. "The Development and Evaluation of the Earth Gravitational Model 2008 (EGM2008)." *Journal of Geophysical Research: Solid Earth* 117 (B4). <https://doi.org/10.1029/2011JB008916>.
- Poudel, K. P., and Q. V. Cao. 2013. "Evaluation of Methods to Predict Weibull Parameters for Characterizing

- Diameter Distributions.” *Forest Science* 59 (2): 243–252. <https://doi.org/10.5849/FORSCI.12-001>.
- Purinton, B., and B. Bookhagen. 2021. “Beyond Vertical Point Accuracy: Assessing Inter-Pixel Consistency in 30 M Global DEMs for the Arid Central Andes.” *Frontiers in Earth Science* 9:901. <https://doi.org/10.3389/feart.2021.758606>.
- Rabby, Y. W., A. Ishtiaque, and M. S. Rahman. 2020. “Evaluating the Effects of Digital Elevation Models in Landslide Susceptibility Mapping in Rangamati District, Bangladesh.” *Remote Sensing* 12 (17): 2718. <https://doi.org/10.3390/RS12172718>.
- Rabus, B., M. Eineder, A. Roth, and R. Bamler. 2003. “The Shuttle Radar Topography Mission—A New Class of Digital Elevation Models Acquired by Spaceborne Radar.” – *ISPRS Journal of Photogrammetry and Remote Sensing* 57 (4): 241–262. [https://doi.org/10.1016/S0924-2716\(02\)00124-7](https://doi.org/10.1016/S0924-2716(02)00124-7).
- Rao, B. S., G. A. Kumar, P. V. S. S. N. Gopala Krishna, P. Srinivasulu, and V. Raghu Venkataraman. 2012. “Evaluation of EGM 2008 with EGM96 and Its Utilization in Topographical Mapping Projects.” *The Journal of the Indian Society of Remote Sensing* 40 (2): 335–340. <https://doi.org/10.1007/s12524-011-0131-1>.
- Roman, D. R., Y. M. Wang, and J. Saleh. 2010. “TS 1C-Geodetic Infrastructure and Datum Geodesy, Geoids, and Vertical Datums: A Perspective from the U.S. National Geodetic Survey.”
- R Project. 2022. “The R Project for Statistical Computing.” <https://www.r-project.org/>.
- Sánchez, J. O. R., J. E. M. Serrano, M. P. J. Páz, N. R. Serrato, and N. L. Váldez. 2022. “Morphometric Analysis of Volcanic Structures Using Digital Elevation Models and Models Developed from Radar Images in the Apan Volcanic Field, México.” <https://doi.org/10.5194/EGUSPHERE-EGU22-10780>.
- Schlaffer, S., P. Matgen, M. Hollaus, and W. Wagner. 2015. “Flood Detection from Multi-Temporal SAR Data Using Harmonic Analysis and Change Detection.” *International Journal of Applied Earth Observation and Geoinformation* 38:15–24. <https://doi.org/10.1016/J.JAG.2014.12.001>.
- Sinem Ince, E., F. Barthelmes, S. Reißland, K. Elger, C. Förste, F. Flechtner, and H. Schuh. 2019. “ICGEM – 15 Years of Successful Collection and Distribution of Global Gravitational Models, Associated Services, and Future Plans.” *Earth System Science Data* 11 (2): 647–674. <https://doi.org/10.5194/ESSD-11-647-2019>.
- Stevens, N. F., V. Manville, and D. W. Heron. 2003. “The Sensitivity of a Volcanic Flow Model to Digital Elevation Model Accuracy: Experiments with Digitised Map Contours and Interferometric SAR at Ruapehu and Taranaki Volcanoes, New Zealand.” *Journal of Volcanology and Geothermal Research* 119 (1–4): 89–105. [https://doi.org/10.1016/S0377-0273\(02\)00307-4](https://doi.org/10.1016/S0377-0273(02)00307-4).
- Sun, G., K. J. Ranson, D. S. Kimes, J. B. Blair, and K. Kovacs. 2008. “Forest Vertical Structure from GLAS: An Evaluation Using LVIS and SRTM Data.” *Remote Sensing of Environment* 112 (1): 107–117. <https://doi.org/10.1016/J.RSE.2006.09.036>.
- Takaku, J., T. Tadono, K. Tsutsui, and M. Ichikawa. 2015. “Quality Status of High Resolution Global DSM Generated from ALOS PRISM.” Paper presented at the IEEE International Geoscience and Remote Sensing Symposium (IGARSS), Milan, July 26–31.
- Tsyganskaya, V., S. Martinis, A. Twele, W. Cao, A. Schmitt, P. Marzahn, and R. Ludwig. 2016. “A Fuzzy Logic-based Approach for the Detection of Flooded Vegetation by Means of Synthetic Aperture Radar Data.” *The International Archives of the Photogrammetry, Remote Sensing and Spatial Information Sciences* XLI-B7:371–378. <https://doi.org/10.5194/ISPRS-ARCHIVES-XLI-B7-371-2016>.
- Üstün, A., R. A. Abbak, and E. Z. Öztürk. 2016. “Height Biases of SRTM DEM Related to EGM96: From a Global Perspective to Regional Practice.” *Survey Review* 50 (358): 26–35. <https://doi.org/10.1080/00396265.2016.1218159>.
- Uuemaa, E., S. Ahi, B. Montibeller, M. Muru, and A. Kmoch. 2020. “Vertical Accuracy of Freely Available Global Digital Elevation Models (ASTER, AW3D30, MERIT, TanDEM-X, SRTM, and NASADEM).” *Remote Sensing* 12 (21): 3482. <https://doi.org/10.3390/rs12213482>.
- Valle, H. D., F. Tentor, W. Sione, P. Zamboni, P. Acenolaza, and G. Metternicht. 2022. “Vertical Accuracy Assessment of Freely Available Digital Elevation Models: Implications for Low-Relief Landscapes.” Paper presented at the International Geoscience and Remote Sensing Symposium (IGARSS), Kuala Lumpur, July 17–22.
- Wessel, B., M. Huber, C. Wohlfart, U. Marschalk, D. Kosmann, and A. Roth. 2018. “Accuracy Assessment of the Global TanDEM-X Digital Elevation Model with GPS Data.” *Isprs Journal of Photogrammetry & Remote Sensing* 139:171–182. <https://doi.org/10.1016/J.ISPRSIPRS.2018.02.017>.
- Willmott, C. J., and K. Matsuura. 2005. “Advantages of the Mean Absolute Error (MAE) Over the Root Mean Square Error (RMSE) in Assessing Average Model Performance.” *Climate Research* 30 (1): 79–82. <https://doi.org/10.3354/CR030079>.
- Wise, S. 2000. “Assessing the Quality for Hydrological Applications of Digital Elevation Models Derived from Contours.” *Hydrological Processes* 14:1909–1929. [https://doi.org/10.1002/1099-1085\(20000815/30\)14:11/12<1909:AID-HYP45>3.0.CO;2-6](https://doi.org/10.1002/1099-1085(20000815/30)14:11/12<1909:AID-HYP45>3.0.CO;2-6).
- WRM (World Rainforest Movement). 2013. “Gabon: New Study Warns of Impacts of the Expansion of Oil Palm and Rubber Tree Plantations.” *WRM Bulletin* 187. <https://www.wrm.org.uy/bulletin-articles/gabon-new-study-warns-of-impacts-of-the-expansion-of-oil-palm-and-rubber-tree-plantations>.
- Xu, K., J. Fang, Y. Fang, Q. Sun, C. Wu, and M. Liu. 2021. “The Importance of Digital Elevation Model Selection in Flood Simulation and a Proposed Method to Reduce DEM Errors: A Case Study in Shanghai.” *International Journal of Disaster Risk Science* 12 (6): 890–902. <https://doi.org/10.1007/s13753-021-00377-z>.
- Yan, L., J. Wang, and D. Shao. 2022. “Glacier Mass Balance in the Manas River Using Ascending and Descending Pass of Sentinel 1A/1B Data and SRTM DEM.” *Remote Sensing* 14 (6): 1506. <https://doi.org/10.3390/RS14061506>.